

LGP2 is a positive regulator of RIG-I- and MDA5-mediated antiviral responses

Takashi Satoh^{a,1}, Hiroki Kato^{a,1,2}, Yutaro Kumagai^a, Mitsutoshi Yoneyama^{b,c}, Shintaro Sato^{a,3}, Kazufumi Matsushita^a, Toru Tsujimura^d, Takashi Fujita^b, Shizuo Akira^{a,4}, and Osamu Takeuchi^a

^aLaboratory of Host Defense, WPI Immunology Frontier Research Center, Research Institute for Microbial Diseases, Osaka University, Osaka 565-0871, Japan; ^bDepartment of Genetics and Molecular Biology, Institute for Virus Research, and Laboratory of Molecular Cell Biology, Graduate School of Biostudies, Kyoto University, Kyoto 606-8507, Japan; ^cPRESTO, Japan Science and Technology Agency, Saitama, Japan; and ^dDepartment of Pathology, Hyogo College of Medicine, Hyogo 663-8501, Japan

Contributed by Shizuo Akira, November 10, 2009 (sent for review October 30, 2009)

RNA virus infection is recognized by retinoic acid-inducible gene (RIG)-I-like receptors (RLRs), RIG-I, and melanoma differentiation-associated gene 5 (MDA5) in the cytoplasm. RLRs are comprised of N-terminal caspase-recruitment domains (CARDs) and a DExD/H-box helicase domain. The third member of the RLR family, LGP2, lacks any CARDs and was originally identified as a negative regulator of RLR signaling. In the present study, we generated mice lacking LGP2 and found that LGP2 was required for RIG-I- and MDA5-mediated antiviral responses. In particular, LGP2 was essential for type I IFN production in response to picornaviridae infection. Overexpression of the CARDs from RIG-I and MDA5 in *Lgp2*^{-/-} fibroblasts activated the IFN- β promoter, suggesting that LGP2 acts upstream of RIG-I and MDA5. We further examined the role of the LGP2 helicase domain by generating mice harboring a point mutation of Lys-30 to Ala (*Lgp2*^{K30A/K30A}) that abrogated the LGP2 ATPase activity. *Lgp2*^{K30A/K30A} dendritic cells showed impaired IFN- β productions in response to various RNA viruses to extents similar to those of *Lgp2*^{-/-} cells. *Lgp2*^{-/-} and *Lgp2*^{K30A/K30A} mice were highly susceptible to encephalomyocarditis virus infection. Nevertheless, LGP2 and its ATPase activity were dispensable for the responses to synthetic RNA ligands for MDA5 and RIG-I. Taken together, the present data suggest that LGP2 facilitates viral RNA recognition by RIG-I and MDA5 through its ATPase domain.

innate immunity | type I interferon | virus infection

RNA virus infection is initially recognized by host pattern recognition receptors, including retinoic acid-inducible gene (RIG)-I-like receptors (RLRs) and Toll-like receptors (TLRs), which induce antiviral responses such as the productions of type I IFNs and proinflammatory cytokines (1–4). The RLR family comprises RIG-I, melanoma differentiation-associated gene 5 (MDA5) and LGP2. RLRs harbor a central DExD/H-box helicase domain and a C-terminal regulatory domain (RD). RIG-I and MDA5 also contain two N-terminal caspase recruitment domains (CARDs), whereas LGP2 does not. RIG-I recognizes relatively short double-stranded (ds) RNAs (up to 1 kb), and the presence of a 5' triphosphate end greatly potentiates its type I IFN-inducing activity (5–7). On the other hand, MDA5 detects long dsRNAs (more than 2 kb), such as polyinosinic polycytidylic acid (poly I:C). Analyses of *Rig-I*-deficient (*Rig-I*^{-/-}) and *Mda5*^{-/-} mice have shown that RIG-I is essential for the production of type I IFNs in response to various RNA viruses, including vesicular stomatitis virus (VSV), Sendai virus (SeV), Japanese encephalitis virus (JEV), and influenza virus, whereas MDA5 is critical for the detection of picornaviridae such as encephalomyocarditis virus (EMCV) and mengovirus (8, 9). Some RNA viruses such as West Nile virus and reovirus are recognized by both RIG-I and MDA5 (10, 11). RIG-I is also reported to be involved in the recognition of foreign DNA in the cytoplasm through transcription of the DNA to dsRNA by polymerase III (12, 13).

The C-terminal RDs of RLRs are responsible for binding to dsRNAs (3). However, the functions of the helicase domains of the RLR family members have not yet been clarified. Although

the RIG-I helicase domain has the ability to unwind dsRNA, this activity is not correlated with the level of IFN production (14). A recent report proposed that the RIG-I ATPase activity is required for translocation of RIG-I on dsRNA (15). The N-terminal CARDs of RIG-I and MDA5 trigger intracellular signaling pathways via IFN- β promoter stimulator (IPS)-1 (also known as MAVS, VISA, or CARDIF), an adaptor molecule possessing an N-terminal CARD (16). IPS-1 subsequently activates two I κ B kinase (IKK)-related kinases, IKK- β , and TANK-binding kinase 1 (TBK1). These kinases phosphorylate IFN-regulatory factor (IRF) 3 and IRF7, which activate the transcription of genes encoding type I IFNs and IFN-inducible genes. The produced type I IFNs alert the surrounding cells by triggering signaling cascades that lead to phosphorylation and nuclear translocation of STAT1 (1, 2).

The third RLR family member LGP2, also known as Dhx58, harbors a DExD/H-box helicase domain and a C-terminal RD but lacks any CARDs (17). In vitro studies have suggested that LGP2 negatively regulates RIG-I-mediated dsRNA recognition (18). Several models have been proposed for the mechanisms of this inhibition. The first model is that LGP2 binds to viral dsRNA and prevents RIG-I- and MDA5-mediated recognition (18). The second model is that LGP2 inhibits multimerization of RIG-I and its interaction with IPS-1 via the RD of LGP2 (19). The third model is that LGP2 competes with IKK- β for recruitment to IPS-1, thereby suppressing RLR signaling (20). Structural analyses of the C-terminal domain of LGP2 have revealed that LGP2 can bind to the termini of dsRNAs more firmly than MDA5 (21–23). A previous report showed that *Lgp2*^{-/-} mice exhibit enhanced production of type I IFNs in response to poly I:C stimulation and VSV infection, whereas the response to EMCV is suppressed (24). Therefore, the role of LGP2 in the negative or positive regulation of RLR signaling has not yet been fully clarified.

In the present study, we generated *Lgp2*^{-/-} mice and mice harboring a point mutation in the LGP2 helicase domain (K30A), and examined their responses to RNA viruses recognized by RIG-I and MDA5. Conventional dendritic cells (cDCs) and mouse embryonic fibroblasts (MEFs) obtained from *Lgp2*^{-/-} mice showed severely impaired IFN responses to infections with picornaviruses, which are recognized by MDA5. Furthermore,

Author contributions: T.S., H.K., S.A., and O.T. designed research; T.S., H.K., Y.K., S.S., K.M., and T.T. performed research; M.Y. and T.F. contributed new reagents/analytic tools; T.S., H.K., T.T., S.A., and O.T. analyzed data; and S.A. and O.T. wrote the paper.

The authors declare no conflict of interest.

See Commentary on page 1261.

¹T.S. and H.K. contributed equally to this work.

²Present address: Program in Molecular Medicine, University of Massachusetts, Worcester, MA 01605.

³Present address: Division of Mucosal Immunology, Department of Microbiology and Immunology, Institute of Medical Science, University of Tokyo, Tokyo 108-8639, Japan.

⁴To whom correspondence should be addressed. E-mail: sakira@biken.osaka-u.ac.jp.

This article contains supporting information online at www.pnas.org/cgi/content/full/0912986107/DCSupplemental.

the responses to viruses recognized by RIG-I were also impaired in *Lgp2*^{-/-} cells. In contrast, the IFN productions in response to synthetic RNAs, poly I:C and RNA synthesized by T7 polymerase, were comparable between wild-type (WT) and *Lgp2*^{-/-} or *Lgp2*^{K30A/K30A} cells. *Lgp2*^{-/-} and *Lgp2*^{K30A/K30A} mice were highly susceptible to infection with EMCV. Taken together, the present results demonstrate that LGP2 acts as a positive, but not negative, regulator of RIG-I- and MDA5-mediated viral recognition.

Results

Generation of Mice Lacking Lgp2. To investigate the physiological role of LGP2 in vivo, we established *Lgp2*^{-/-} mice (Fig. S1A and B). As reported previously, the expression of *Lgp2* mRNA was highly induced in response to IFN- β stimulation in MEFs (Fig. S1C) (17). Expression of *Lgp2* mRNA was not detected in *Lgp2*^{-/-} MEFs, whereas the expression levels of *Rig-I* and *Mda5* mRNAs were comparable between WT and *Lgp2*^{-/-} cells (Fig. S1C). The *Lgp2*^{-/-} progenies obtained from *Lgp2*^{+/-} intercrosses were lower than the expected Mendelian ratio (Fig. S2A), indicating that homozygous mutations of the *Lgp2* gene cause embryonic lethality at a high frequency. In addition, adult female *Lgp2*^{-/-} mice showed an enlarged uterus filled with fluid resulting from vaginal atresia (Fig. S2B and C).

Role of LGP2 in Type I IFN and Cytokine Productions in Response to RNA Viruses. First, we examined the production of IFN- β in cDCs derived from bone marrow (BM) in the presence of GM-CSF after infection with a variety of RNA viruses (Fig. 1). The productions of IFN- β in response to picornaviridae, EMCV, and mengovirus were severely impaired in *Lgp2*^{-/-} cDCs compared

with WT cells (Fig. 1A). IL-6 production induced by EMCV infection was also severely impaired in *Lgp2*^{-/-} cells (Fig. 1B). Furthermore, LGP2 was involved in the productions of IFN- β in response to several RNA viruses recognized by RIG-I, such as VSV, SeV, and JEV (Fig. 1A). IFN- β production in response to reovirus, a dsRNA virus, was also impaired in *Lgp2*^{-/-} cells (Fig. 1A). In contrast, the IFN- β productions in response to infection with influenza virus were comparable between WT and *Lgp2*^{-/-} cDCs (Fig. 1A). Stimulation with CpG-DNA, a TLR9 ligand, induced comparable amounts of IFN- β in WT and *Lgp2*^{-/-} cells (Fig. 1A).

Next, we examined whether the defect in type I IFN production in response to EMCV was controlled at the mRNA level. The expressions of the genes encoding IFN- β , CXCL10 and IL-6 after infection with EMCV were severely impaired in *Lgp2*^{-/-} macrophages (Fig. 2A). However, the influenza virus-induced expressions of IFN- β and CXCL10 mRNAs were comparable between WT and *Lgp2*^{-/-} MEFs throughout the whole time course (Fig. 2B). Therefore, it is unlikely that LGP2 negatively regulates RIG-I-mediated responses, even during the later period of infection. These results indicate that LGP2 is involved in positive, but not negative, regulation of virus recognition by MDA5 and RIG-I, with the exception of influenza virus.

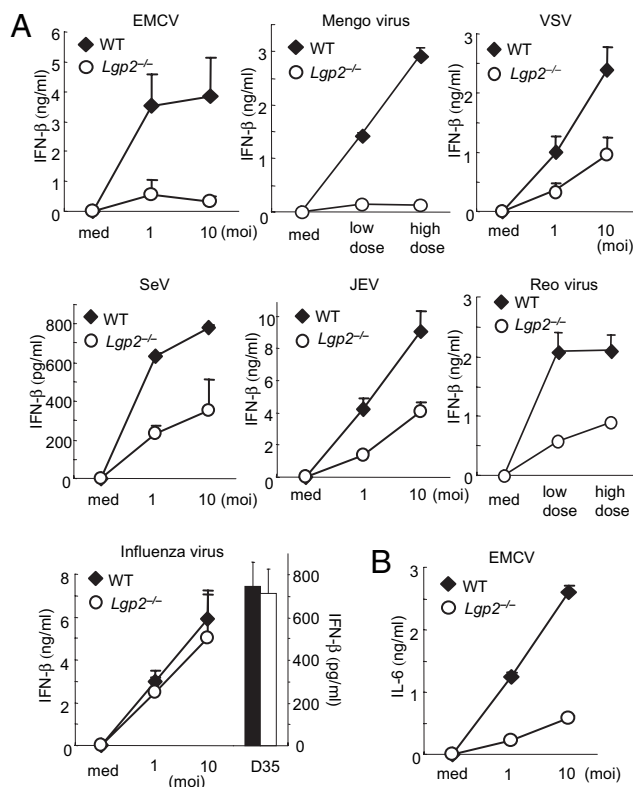


Fig. 1. Role of LGP2 in type I IFN production in response to various RNA viruses. (A and B) BM-derived cDCs from WT and *Lgp2*^{-/-} mice were exposed to the indicated viruses or treated with 1 μ M CpG-DNA (D35) for 24 h. The concentrations of IFN- β (A) and IL-6 (B) in the culture supernatants were measured by ELISA. moi, multiplicity of infection; med, medium alone. Data are shown as means \pm SD and are representative of at least three independent experiments.

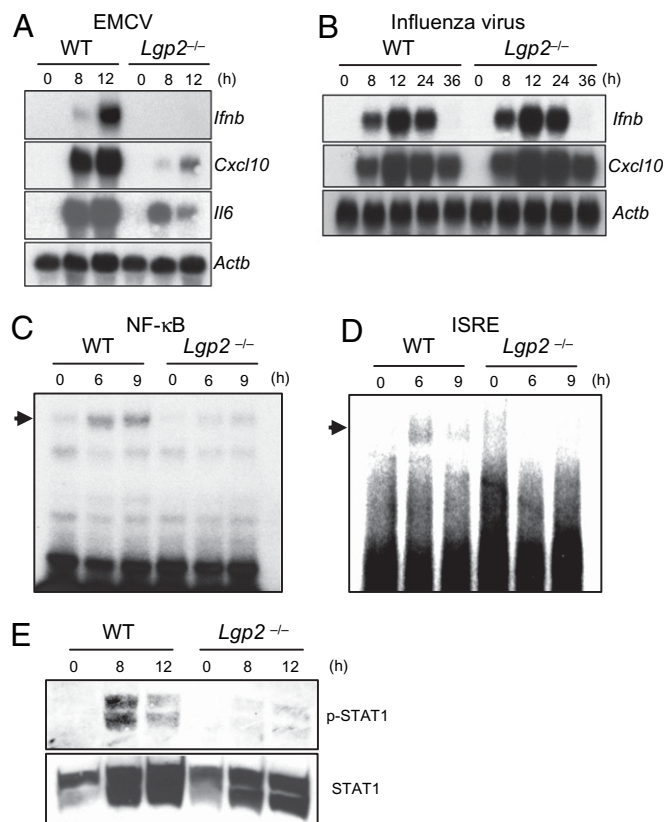


Fig. 2. Role of LGP2 in the activation of signaling pathways leading to IFN-inducible gene expression. (A) Total RNAs extracted from WT and *Lgp2*^{-/-} macrophages infected with EMCV were subjected to Northern blot analyses for the expressions of *Ifnb*, *Cxcl10*, *Il6*, and *Actb* mRNAs. (B) WT and *Lgp2*^{-/-} MEFs were infected with influenza virus followed by isolation of the total RNA. The expressions of *Ifnb*, *Cxcl10*, and *Actb* mRNAs were determined by Northern blot analyses. (C and D) Nuclear extracts were prepared from WT and *Lgp2*^{-/-} macrophages infected with EMCV for the indicated periods. The binding activities of DNA to NF- κ B (C) and ISREs (D) were determined by EMSAs. (E) Cell lysates were prepared from WT and *Lgp2*^{-/-} macrophages infected with EMCV and probed with anti-phospho-STAT1 and anti-STAT1 antibodies. The data are representative of at least three independent experiments.

Cell Type-Specific Involvement of LGP2 in EMCV Recognition. We previously showed that RIG-I- and MDA5-dependent RNA virus recognition occurs in cDCs but not in plasmacytoid dendritic cells (pDCs) (8). To determine whether LGP2 functions in a cell type-specific fashion, B220⁺CD11c⁺ cDCs and CD11c⁺B220⁺ pDCs were purified from WT and *Lgp2*^{-/-} splenocytes. EMCV-induced IFN- β production was severely impaired in *Lgp2*^{-/-} splenic cDCs compared with WT cDCs, whereas splenic pDCs from WT and *Lgp2*^{-/-} mice produced comparable amounts of IFN- β (Fig. S3). These data indicate that LGP2 functions in cDCs but not in pDCs.

LGP2 Is Essential for Triggering RLR Signaling Pathways. To investigate whether LGP2 regulates the primary responses to RNA virus infections, we examined the activation of intracellular signaling pathways. Electrophoretic mobility shift assays (EMSA) revealed that the activations of NF- κ B and IFN-stimulated regulatory elements (ISREs) in response to EMCV infection were severely impaired in *Lgp2*^{-/-} cells (Fig. 2C and D). Furthermore, the phosphorylation of STAT1 was abrogated in *Lgp2*^{-/-} cells (Fig. 2E). Nevertheless, the expressions of *Lgp2* in response to IFN- β treatment were not altered in *Rig-I*^{-/-} and *Mda5*^{-/-} cells (Fig. S4). These results suggest that LGP2 is required for the initial recognition of EMCV, leading to activation of transcription factors involved in the expression of type I IFNs.

Next, we examined whether the expression of *Lgp2* could rescue the virus-mediated IFN responses. IFN- β -dependent reporter gene expression was induced in response to EMCV infection in WT, but not in *Lgp2*^{-/-} MEFs (Fig. 3A). Expression of exogenous LGP2 in *Lgp2*^{-/-} cells restored the EMCV-induced IFN- β promoter activity as well as IFN- β production (Fig. 3A and B). Although overexpression of either LGP2 or MDA5 alone in *Lgp2*^{-/-}*Mda5*^{-/-} MEFs failed to confer EMCV-induced IFN- β promoter activity, coexpression of both LGP2 and MDA5 restored EMCV responsiveness (Fig. 3C). Overexpression of the CARDS from RIG-I or MDA5 in *Lgp2*^{-/-} MEFs activated the IFN- β promoter (Fig. 3D), suggesting that LGP2 functions upstream of RIG-I and MDA5.

Normal IFN Responses of LGP2^{-/-} cells to Exogenously Transfected RNAs. We examined the responses of *Lgp2*^{-/-} cells to synthetic RNAs recognized by RIG-I and MDA5. Unexpectedly, WT and *Lgp2*^{-/-} cDCs produced comparable amounts of IFN- β in response to poly I:C, in vitro-transcribed dsRNA and RNA with a 5' triphosphate end (Tri-P) (Fig. 4A). Similarly, *Lgp2*-deficiency did not affect the IFN- β productions in response to the synthesized RNAs in fibroblasts (Fig. 4A). In addition, no differences were observed in the responses to the various concentrations of poly I:C examined (Fig. 4B). These data suggest that LGP2 is dispensable for the recognition of synthesized dsRNA and 5' triphosphate RNA.

Function of LGP2 ATPase Domain in Type I IFN Responses to Virus Infections. The recognition of dsRNA and RNA viruses by RIG-I or MDA5 requires ATPase activity (17, 25). To examine the role of the LGP2 ATPase activity in LGP2-mediated virus recognition, we reconstituted *Lgp2*^{-/-} MEFs with WT LGP2 or LGP2-K30A harboring a Lys-to-Ala point mutation in the Walker ATP-binding motif using a retrovirus system. Expression of WT LGP2 in *Lgp2*^{-/-} MEFs conferred IFN- β promoter activity as well as IFN- β production in response to EMCV, whereas expression of LGP2-K30A failed to confer these responses to EMCV infection (Fig. 5A and B).

To further examine the role of the LGP2 ATPase activity in vivo, we generated mice harboring the LGP2 K30A point mutation (Fig. S5A and B). Expression of *Lgp2* mRNA was comparably induced in response to IFN- β stimulation in WT and *Lgp2*^{K30A/K30A} MEFs (Fig. S5C). We confirmed the insertion of

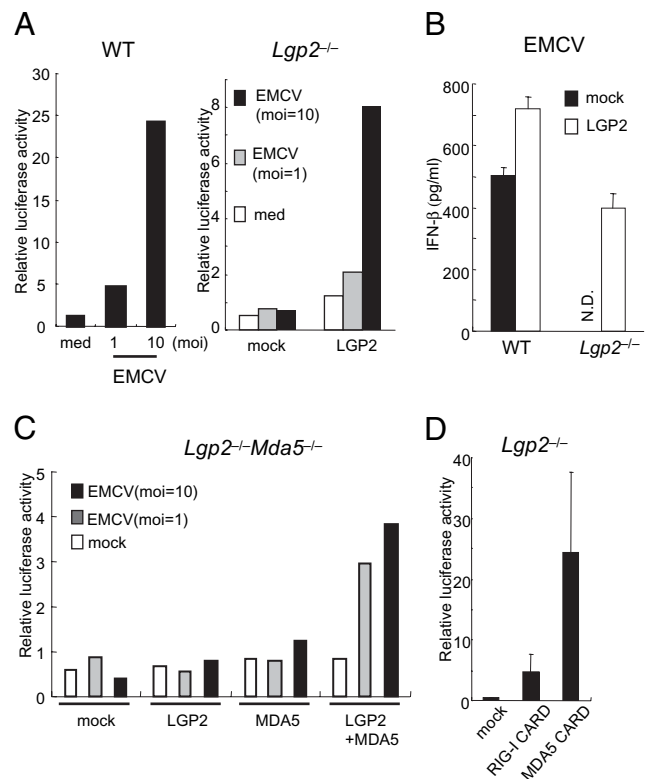


Fig. 3. LGP2 acts in the upstream of RIG-I and MDA5. (A) WT and *Lgp2*^{-/-} MEFs were transiently transfected with the IFN- β promoter construct together with expression plasmids encoding LGP2. The cells were infected with EMCV for 8 h and then lysed. The cell lysates were analyzed by a luciferase assay. (B) WT and *Lgp2*^{-/-} MEFs were infected with a retrovirus expressing *Lgp2*. At 2 days after infection, the cells were exposed to EMCV for 24 h. The IFN- β concentrations in the culture supernatants were measured by ELISA. N.D., not detected. (C) *Lgp2*^{-/-}*Mda5*^{-/-} MEFs were transiently transfected with the IFN- β promoter reporter construct together with the indicated expression plasmids. After 24 h, the cells were infected with EMCV for 8 h and then lysed. The cell lysates were analyzed by a luciferase assay. (D) *Lgp2*^{-/-} MEFs were transiently transfected with the IFN- β promoter construct together with expression plasmids encoding the CARDS of RIG-I or MDA5 and then lysed at 48 h after transfection. The cell lysates were analyzed by a luciferase assay.

the point mutation by sequencing analysis (Fig. S5D). The *Lgp2*^{K30A/K30A} mice were born at the expected Mendelian ratio, and did not show any developmental defects. We examined the IFN- β productions in cDCs in response to infections with RNA viruses. The IFN- β productions in response to infections with EMCV, mengovirus, VSV, SeV, and reovirus, but not with influenza virus, were severely impaired in *Lgp2*^{K30A/K30A} cDCs compared with WT cells (Fig. 5C). The IL-6 production in response to EMCV infection was also impaired in *Lgp2*^{K30A/K30A} cDCs (Fig. 5D). The defects observed in *Lgp2*^{K30A/K30A} cDCs were as severe as those observed in *Lgp2*^{-/-} cDCs, suggesting that the ATPase activity of LGP2 is essential for the recognition of viruses. The productions of IFN- β in response to transfections of synthetic RNAs and poly I:C were comparable between WT and *Lgp2*^{K30A/K30A} cells (Fig. 5E), further confirming that LGP2 is not involved in the responses to the transfection of synthetic RNAs. Taken together, these results indicate that the ATPase activity of LGP2 is essential for LGP2 to function as a positive regulator in MEFs. This finding is in marked contrast to in vitro experiments in which overexpression of WT LGP2 and LGP2-K30A in HEK293 cells suppressed RIG-I-mediated IFN- β promoter activity (Fig. S6), suggesting that overexpression of

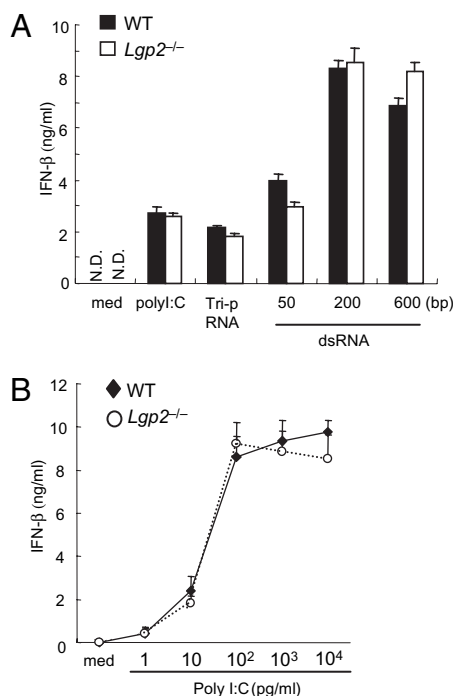


Fig. 4. Role of LGP2 in the recognition of exogenously transfected RNAs. (A) WT and *Lgp2*^{-/-} MEFs were stimulated with triphosphate RNA, in vitro-transcribed dsRNA (1 μg/mL) or poly I:C complexed with Lipofectamine 2000 for 24 h. The IFN-β concentrations in the culture supernatants were measured by ELISA. med, medium; N.D., not detected. Data are shown as the means ± SD of triplicate samples. Similar results were obtained in three independent experiments. (B) WT and *Lgp2*^{-/-} MEFs were transfected with the indicated amounts of poly I:C complexed with Lipofectamine 2000. The IFN-β concentrations in the culture supernatants were measured by ELISA.

LGP2 in HEK293 cells nonspecifically inhibits the RIG-I-mediated pathway.

Role of LGP2 and Its ATPase Activity in Antiviral Host Defenses In Vivo. Finally, we assessed the role of LGP2 and its ATPase activity in antiviral responses in vivo. When *Lgp2*^{-/-} mice were challenged with EMCV, IFN-β production was not detected in their sera (Fig. 6A). Furthermore, *Lgp2*^{-/-} mice were highly susceptible to EMCV infection compared with their littermate controls (Fig. 6C). Consistent with the increased susceptibility to EMCV, the viral titer in the heart was remarkably higher in *Lgp2*^{-/-} mice than in control mice (Fig. 6E). Similar to the results for *Lgp2*^{-/-} mice, *Lgp2*^{K30A/K30A} mice showed severe defects in IFN-β production in response to EMCV infection (Fig. 6B). *Lgp2*^{K30A/K30A} mice were highly susceptible to infection with EMCV, with highly increased viral titers in their hearts (Fig. 6D and F). These data indicate that LGP2 also plays a key role in the host defenses against RNA viruses recognized by MDA5 in vivo.

Discussion

The present data clearly demonstrate that LGP2 acts as a positive regulator of MDA5- and RIG-I-mediated viral recognition, except for influenza virus. These findings are in contrast to the conclusions deduced from previous in vitro studies and a report on *Lgp2* knockout mice generated by another group (17, 18, 20, 24). LGP2 is particularly important for the recognition of picornaviruses, including EMCV and mengovirus, among RNA viruses. Analyses of the activation status of signaling molecules revealed that LGP2 was involved in the primary recognition of EMCV upstream of MDA5. LGP2 was also involved in the recognition of RNA viruses recognized by RIG-I, such as VSV

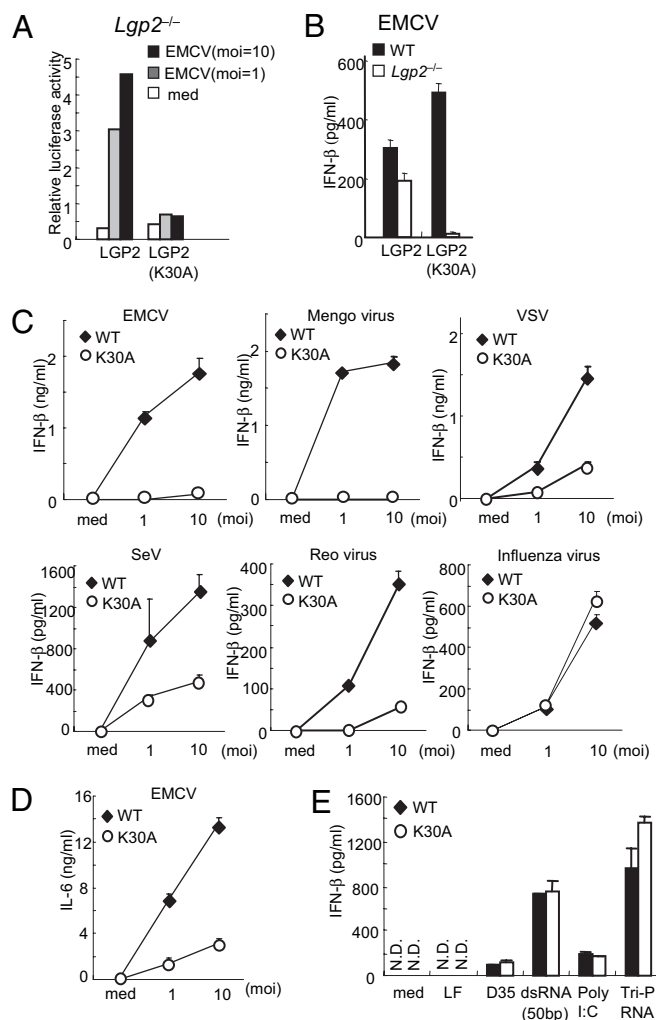


Fig. 5. Essential role of the LGP2 ATPase activity in the recognition of RNA viruses. (A) *Lgp2*^{-/-} MEFs were transiently transfected with the IFN-β promoter construct together with expression plasmids encoding *LGP2* or *LGP2* (K30A). The cells were infected with EMCV for 8 h and then lysed. The cell lysates were analyzed by a luciferase assay. (B) WT and *Lgp2*^{-/-} MEFs were infected with retroviruses expressing *LGP2* or *LGP2* (K30A). At 2 days after infection, the cells were exposed to EMCV for 24 h and the IFN-β concentrations in the culture supernatants were measured by ELISA. (C and D) WT and *Lgp2*^{K30A/K30A} (K30A) mice were exposed to the indicated RNA viruses for 24 h. The concentrations of IFN-β (C) and IL-6 (D) in the culture supernatants were measured by ELISA. (E) WT and *Lgp2*^{K30A/K30A} cDCs were transfected with the indicated RNAs for 24 h. The concentrations of IFN-β in the culture supernatants were measured by ELISA. moi, multiplicity of infection; med, medium alone; LF, lipofectamine alone. Data are shown as means ± SD and are representative of at least three independent experiments.

and SeV, although the defects in the responses to these viruses observed in *Lgp2*^{-/-} cells were not as severe as the defects in the responses to picornaviruses. Surprisingly, *Lgp2*^{-/-} cells responded efficiently to synthetic RNA compounds, including poly I:C, dsRNA transcribed in vitro using T7 polymerase and 5' triphosphate RNA.

Cells from *Lgp2*^{K30A/K30A} mice showed severe defects in the IFN responses to RNA viruses to extents similar to those of *Lgp2*^{-/-} cells. Furthermore, expression of the LGP2-K30A mutant protein in *Lgp2*^{-/-} cells failed to restore the EMCV responsiveness. These results clearly demonstrate that the ATPase domain of LGP2 is a prerequisite for its function in recognizing RNA virus infection. Recent advances in studies on DExD/H-box

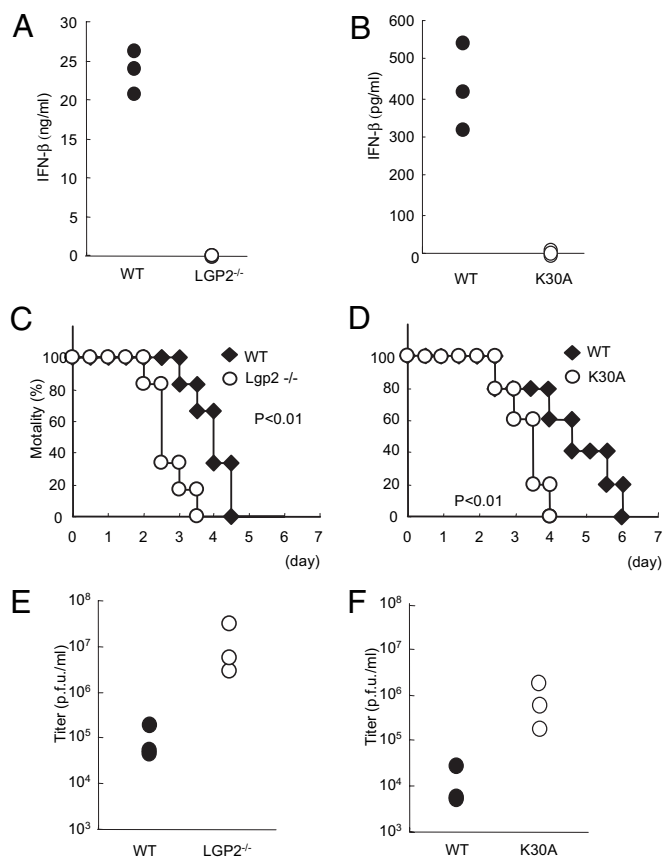


Fig. 6. Role of LGP2 in host defense against EMCV infection in vivo. (A and B) WT and littermate *Lgp2*^{-/-} mice (A) or WT and littermate *Lgp2*^{K30A/K30A} (K30A) mice (B) were i.v. inoculated with 1×10^7 pfu EMCV. Serum samples were obtained at 4 h after injection, and the IFN- β concentrations were determined by ELISA. (C and D) Survival rates of WT and *Lgp2*^{-/-} mice (C) or WT and littermate *Lgp2*^{K30A/K30A} mice (D) intraperitoneally infected with 1×10^2 pfu EMCV were monitored every 12 h for 5 days. (E and F) WT and littermate *Lgp2*^{-/-} mice (E) or WT and littermate *Lgp2*^{K30A/K30A} mice (F) were infected i.p. with 1×10^2 pfu EMCV. After 48 h, the mice were killed and the virus titers in their hearts were determined by a plaque assay.

proteins have revealed that these proteins are involved in all aspects of RNA metabolism including translation initiation, mRNA splicing, and nuclear transport (26). Although DEXD/H-box proteins, including RIG-I, are known to exhibit ATP-dependent RNA helicase activity in vitro, many DEXD/H-box proteins have a more general RNA conformational change activity, rather than just a duplex-unwinding activity. In this regard, it is tempting to speculate that LGP2 functions to modify viral RNA by removing proteins from viral ribonucleoprotein (RNP) complexes or unwinding complex RNA structures to facilitate MDA5- and RIG-I-mediated recognition of dsRNA. Picornaviruses replicate in association with the cytoplasmic membranes of infected cells (27). It is therefore possible that LGP2 makes viral RNP complexes more accessible to MDA5 and RIG-I by changing their intracellular localization.

RLLRs contain a C-terminal regulatory domain that is responsible for the binding to dsRNAs. The recent solution of the RLLR C-terminal regulatory domain structures showed that the LGP2 and RIG-I C-terminal domains have a large basic surface, formed by the RNA-binding loop, and that the LGP2 C-terminal domain binds to the termini of dsRNAs (14, 21–23, 28). Although the MDA5 C-terminal domain also has a large basic surface, it is extensively flat because of the open conformation of the RNA-binding loop (21). Consequently, the RNA-binding activity of MDA5 is much weaker than those of RIG-I and

LGP2. The present study has demonstrated that LGP2 is more profoundly required for the recognition of RNA viruses detected by MDA5 than for those detected by RIG-I. MDA5 may require LGP2 for efficient recruitment of viral dsRNAs to facilitate the initiation of signaling, and LGP2 appears to be more important for MDA5 than for RIG-I, possibly because of differences in their affinities for dsRNAs.

Although LGP2 is involved in the responses to various RNA viruses, influenza virus infection induced normal type I IFN production in *Lgp2*^{-/-} cells. Type I IFN production in response to influenza virus was dependent on RIG-I but not on MDA5. We (5) and Pichlmair et al. (29) previously showed that phosphatase treatment of genomic RNA derived from influenza virus completely abolishes its type I IFN-inducing activity via RIG-I, indicating that a phosphate group at the 5' end of the influenza virus genome is responsible for RIG-I-mediated recognition. Therefore, the 5' triphosphate RNA present on viral genomes may be readily accessible to RIG-I without modification by LGP2.

Venkataraman et al. (24) reported that LGP2 acts as a negative regulator for the recognition of VSV and poly I:C, and a positive regulator for EMCV-induced IFN responses in macrophages by generating *Lgp2*^{-/-} mice. Their results are contradictory to our present findings in terms of the responses to poly I:C and viruses recognized by RIG-I. Although we do not have a clear explanation for these discrepancies, expression of LGP2 in *Lgp2*^{-/-} cells restored the responses to VSV and EMCV. Furthermore, we found that both *Lgp2*^{-/-} and *Lgp2*^{K30A/K30A} cells showed defects in IFN production in response to certain viruses recognized by RIG-I and showed normal responses to dsRNA specimens. Therefore, we believe that LGP2 acts as a positive, but not negative, regulator of RIG-I- and MDA5-dependent recognition of RNA virus infection and plays a pivotal role in antiviral responses in vivo.

Although some of the female *Lgp2*^{-/-} mice showed a defect in the development of the vagina, *Lgp2*^{K30A/K30A} mice did not exhibit any developmental abnormalities. Although the ATPase domain was essential for antiviral responses, the vaginal atresia was regulated by LGP2 independently of its ATPase activity. Given that *Rig-I*^{-/-} mice showed fetal liver apoptosis at day 13, it will be interesting to analyze the role of the RIG-I ATPase activity in the control of development. Further studies are required to determine the roles of the RLLR family members in controlling mammalian development.

Given that many RLLR signaling molecules are inhibited by viral components, LGP2 may also be a target of the escape mechanisms exerted by various RNA viruses. Future studies aimed at identifying the mechanisms by which LGP2 modifies viral RNP complexes will help us to understand the roles of the innate immune system in intracellular virus recognition, and will lead to the development of new strategies to manipulate antiviral responses.

Materials and Methods

Generation of *Lgp2*^{-/-} and *Lgp2*^{K30A/K30A} Mice. The *Lgp2* gene was isolated from genomic DNA extracted from embryonic stem (ES) cells (GSI-1) by PCR. The targeting vector was constructed by replacing a 4-kb fragment encoding the *Lgp2* ORF (including the DEXH/H box) with a neomycin-resistance gene cassette (*neo*), and inserting herpes simplex virus thymidine kinase (HSV-TK) driven by the PGK promoter into the genomic fragment for negative selection. After the targeting vector was transfected into ES cells, G418 and gancyclovir double-resistant colonies were selected and screened by PCR, and recombination was confirmed by Southern blotting. Homologous recombinants were microinjected into C57BL/6 female mice, and heterozygous F1 progenies were intercrossed to obtain *Lgp2*^{-/-} mice. *Lgp2*^{-/-} and littermate control mice were used for subsequent experiments.

A point mutation was inserted into a genomic fragment harboring the exon encoding Lys-30 of murine *Lgp2* by site-directed mutagenesis (Clontech) to replace this residue with Ala. A targeting vector was constructed with this genomic fragment and electroporated into ES cells. Homologous recombinants were selected and microinjected into C57BL/6 female mice,

and heterozygous F1 progenies were crossed with CAG-Cre transgenic mice to excise the *neo* cassette. Next, the CAG-Cre transgene was removed from *Lgp2^{+/K30A}* mice by crossing the mice with C57BL/6 mice. *Lgp2^{K30A/K30A}* and littermate control mice were used for subsequent experiments.

All animal experiments were carried out with the approval of the Animal Research Committee of the Research Institute for Microbial Diseases (Osaka University).

Mice, Cells, and Reagents. *Rig-1^{-/-}* and *Lgp2^{-/-}Mda5^{-/-}* MEFs were prepared from embryos on 129Sv and C57BL/6 backgrounds derived at 11.5 days post coitum. BM-derived DCs were generated in RPMI medium 1640 containing 10% FCS, 50 mM 2-mercaptoethanol, and 10 ng/mL GM-CSF (PeproTech). pDCs and cDCs were isolated from the spleen by MACS using anti-B220 and anti-CD11c microbeads (Miltenyi Biotech). Poly I:C was purchased from Amersham Biosciences. RNAs were complexed with the cationic lipid Lipofectamine 2000 (Invitrogen) and added to cells. A/D-type CpG-oligodeoxynucleotides (D35) were synthesized by Hokkaido System Science. In vitro-transcribed dsRNA and triphosphate RNA were described previously (5, 9). Antibodies against phospho-STAT1 and STAT1 (Cell Signaling) were used for Western blotting as described previously (8).

Viruses. VSV, VSV lacking an M protein variant (NCP), influenza virus ΔNS1, JEV, EMCV, and mengovirus were described previously (9). SeV lacking V protein (V-) was kindly provided by Dr. A. Kato. Reovirus was kindly provided by Dr. T. Dermody.

Northern Blotting. Total RNA was extracted from peritoneal macrophages infected with EMCV or MEFs infected with influenza virus using TRIzol reagent (Invitrogen). The obtained RNA was electrophoresed, transferred to nylon membranes, and hybridized with various cDNA probes. To detect the expression of *Lgp2* mRNA, a 326-bp fragment (772–1098) was used as a probe.

EMSA. Peritoneal macrophages (3×10^6) were infected with EMCV for various periods. Nuclear extracts were purified from the cells using lysis buffer (10 mM Hepes-KOH pH 7.8, 10 mM KCl, and 10 mM EDTA, pH 8.0), incubated with specific probes for NF- κ B or ISRE DNA-binding sites, electrophoresed, and visualized by autoradiography.

Luciferase Assay. MEFs were transiently transfected with a reporter construct containing the IFN- β promoter together with an empty vector (Mock) or expression constructs for several genes using Lipofectamine 2000. As an internal control, the cells were transfected with a *Renilla* luciferase construct. The transfected cells were left untreated (medium alone) or infected with EMCV for 8 h. The cells were then lysed and subjected to a luciferase assay using a dual-luciferase reporter assay system (Promega) according to the manufacturer's instructions.

Retroviral Expression. Murine LGP2 and LGP2K30A cDNAs were individually cloned into the pLZR-IRES/GFP retroviral vector (30). Retroviruses were produced by transient transfection of the constructs into PlatE cells. MEFs were separately infected with the retroviruses expressing LGP2 and LGP2 (K30A). At 2 days after infection, the cells were exposed to EMCV for 24 h, and the IFN- β concentrations in the culture supernatants were measured by ELISA.

Plaque Assay. At 48 h after EMCV infection, hearts were prepared and homogenized in PBS. The virus titers in the hearts were determined by a standard plaque assay as described previously (9). After centrifugation, the supernatants were serially diluted and added to plates containing HeLa cells. Cells were overlaid with DMEM containing 1% low-melting point agarose and incubated for 48 h. The numbers of plaques were counted.

Measurement of Cytokine Production. Culture supernatants were collected, and the cytokine concentrations were measured using ELISA kits for IFN- β (PBL Biomedical Laboratories) and IL-6 (R&D Systems) according to the manufacturers' instructions.

Statistical Analysis. The statistical significance of differences between groups was determined by Student's *t* test, and survival curves were analyzed by the log-rank test. Values of $P < 0.05$ were considered to indicate statistical significance.

ACKNOWLEDGMENTS. We thank all of the colleagues in our laboratory, E. Kamada for secretarial assistance, and Y. Fujiwara, M. Kumagai, and R. Abe for technical assistance. We thank Drs. A. Kato and T. Dermody for providing viruses. This work was supported by the Special Coordination Funds of the Japanese Ministry of Education, Culture, Sports, Science and Technology, and grants from the Ministry of Health, Labour and Welfare in Japan, the Global Center of Excellence Program of Japan, and the National Institutes of Health (P01 AI070167).

- Akira S, Uematsu S, Takeuchi O (2006) Pathogen recognition and innate immunity. *Cell* 124:783–801.
- Honda K, Takaoka A, Taniguchi T (2006) Type I interferon [corrected] gene induction by the interferon regulatory factor family of transcription factors. *Immunity* 25:349–360.
- Yoneyama M, Fujita T (2008) Structural mechanism of RNA recognition by the RIG-I-like receptors. *Immunity* 29:178–181.
- Takeuchi O, Akira S (2009) Innate immunity to virus infection. *Immunity Rev* 227:75–86.
- Kato H, et al. (2008) Length-dependent recognition of double-stranded ribonucleic acids by retinoic acid-inducible gene-I and melanoma differentiation-associated gene 5. *J Exp Med* 205:1601–1610.
- Schlee M, et al. (2009) Recognition of 5' triphosphate by RIG-I helicase requires short blunt double-stranded RNA as contained in panhandle of negative-strand virus. *Immunity* 31:25–34.
- Schmidt A, et al. (2009) 5'-triphosphate RNA requires base-paired structures to activate antiviral signaling via RIG-I. *Proc Natl Acad Sci USA* 106:12067–12072.
- Kato H, et al. (2005) Cell type-specific involvement of RIG-I in antiviral response. *Immunity* 23:19–28.
- Kato H, et al. (2006) Differential roles of MDA5 and RIG-I helicases in the recognition of RNA viruses. *Nature* 441:101–105.
- Fredericksen BL, Keller BC, Fornek J, Katze MG, Gale M Jr (2008) Establishment and maintenance of the innate antiviral response to West Nile Virus involves both RIG-I and MDA5 signaling through IPS-1. *J Virol* 82:609–616.
- Loo YM, et al. (2008) Distinct RIG-I and MDA5 signaling by RNA viruses in innate immunity. *J Virol* 82:335–345.
- Chiu YH, Macmillan JB, Chen ZJ (2009) RNA polymerase III detects cytosolic DNA and induces type I interferons through the RIG-I pathway. *Cell* 138:576–591.
- Ablasser A, et al. (2009) RIG-I-dependent sensing of poly(dA:dT) through the induction of an RNA polymerase III-transcribed RNA intermediate. *Nat Immunol* 10:1065–1072.
- Takahashi K, et al. (2008) Nonself RNA-sensing mechanism of RIG-I helicase and activation of antiviral immune responses. *Mol Cell* 29:428–440.
- Myong S, et al. (2009) Cytosolic viral sensor RIG-I is a 5'-triphosphate-dependent translocase on double-stranded RNA. *Science* 323:1070–1074.
- Kawai T, et al. (2005) IPS-1, an adaptor triggering RIG-I- and Mda5-mediated type I interferon induction. *Nat Immunol* 6:981–988.
- Yoneyama M, et al. (2005) Shared and unique functions of the DExD/H-box helicases RIG-I, MDA5, and LGP2 in antiviral innate immunity. *J Immunol* 175:2851–2858.
- Rothenfusser S, et al. (2005) The RNA helicase Lgp2 inhibits TLR-independent sensing of viral replication by retinoic acid-inducible gene-I. *J Immunol* 175:5260–5268.
- Saito T, et al. (2007) Regulation of innate antiviral defenses through a shared repressor domain in RIG-I and LGP2. *Proc Natl Acad Sci USA* 104:582–587.
- Komuro A, Horvath CM (2006) RNA- and virus-independent inhibition of antiviral signaling by RNA helicase LGP2. *J Virol* 80:12332–12342.
- Takahashi K, et al. (2009) Solution structures of cytosolic RNA sensor MDA5 and LGP2 C-terminal domains: Identification of the RNA recognition loop in RIG-I-like receptors. *J Biol Chem* 284:17465–17474.
- Li X, et al. (2009) The RIG-I-like receptor LGP2 recognizes the termini of double-stranded RNA. *J Biol Chem* 284:13881–13891.
- Pippig DA, et al. (2009) The regulatory domain of the RIG-I family ATPase LGP2 senses double-stranded RNA. *Nucleic Acids Res* 37:2014–2025.
- Venkataraman T, et al. (2007) Loss of DExD/H box RNA helicase LGP2 manifests disparate antiviral responses. *J Immunol* 178:6444–6455.
- Yoneyama M, et al. (2004) The RNA helicase RIG-I has an essential function in double-stranded RNA-induced innate antiviral responses. *Nat Immunol* 5:730–737.
- Linder P (2006) Dead-box proteins: A family affair—active and passive players in RNP-remodeling. *Nucleic Acids Res* 34:4168–4180.
- Salonen A, Ahola T, Kääriäinen L (2005) Viral RNA replication in association with cellular membranes. *Curr Top Microbiol Immunol* 285:139–173.
- Cui S, et al. (2008) The C-terminal regulatory domain is the RNA 5'-triphosphate sensor of RIG-I. *Mol Cell* 29:169–179.
- Pichlmair A, et al. (2006) RIG-I-mediated antiviral responses to single-stranded RNA bearing 5'-phosphates. *Science* 314:997–1001.
- Ruiz-Vela A, et al. (2001) Transplanted long-term cultured pre-B1 cells expressing calpastatin are resistant to B cell receptor-induced apoptosis. *J Exp Med* 194:247–254.

Structural Basis of HIV-1 Tethering to Membranes by the BST-2/Tetherin Ectodomain

Andreas Hinz,^{1,5} Nolwenn Miguet,^{1,5} Ganesh Natrajan,¹ Yoshiko Usami,² Hikaru Yamanaka,² Patricia Renesto,¹ Bettina Hartlieb,¹ Andrew A. McCarthy,^{1,3} Jean-Pierre Simorre,⁴ Heinrich Göttlinger,² and Winfried Weissenhorn^{1,*}

¹Unit of Virus Host Cell Interactions (UVHCI) UMI 3265 Université Joseph Fourier-EMBL-CNRS, 6 rue Jules Horowitz, 38042 Grenoble, France

²Program in Gene Function and Expression, Program in Molecular Medicine, University of Massachusetts Medical School, Worcester, MA 01605, USA

³EMBL, 6 rue Jules Horowitz, 38042 Grenoble, France

⁴Institut de Biologie Structurale Jean-Pierre Ebel, UMR 5075 CEA-CNRS-UJF, 41 rue Jules Horowitz, 38027 Grenoble Cedex 01, France

⁵These authors contributed equally to this work

*Correspondence: weissenhorn@embl.fr

DOI 10.1016/j.chom.2010.03.005

SUMMARY

The restriction factor BST-2/tetherin contains two membrane anchors employed to retain some enveloped viruses, including HIV-1 tethered to the plasma membrane in the absence of virus-encoded antagonists. The 2.77 Å crystal structure of the BST-2/tetherin extracellular core presented here reveals a parallel 90 Å long disulfide-linked coiled-coil domain, while the complete extracellular domain forms an extended 170 Å long rod-like structure based on small-angle X-ray scattering data. Mutagenesis analyses indicate that both the coiled coil and the N-terminal region are required for retention of HIV-1, suggesting that the elongated structure can function as a molecular ruler to bridge long distances. The structure reveals substantial irregularities and instabilities throughout the coiled coil, which contribute to its low stability in the absence of disulfide bonds. We propose that the irregular coiled coil provides conformational flexibility, ensuring that BST-2/tetherin anchoring both in the plasma membrane and in the newly formed virus membrane is maintained during virus budding.

INTRODUCTION

Enveloped viruses rely on host cell factors to complete their life cycle. These factors act as positive or negative regulators, such as restriction factors, that often limit replication to a narrow range of hosts and cell types (Malim and Emerman, 2008). While restriction factors are inducible by IFN and thus constitute a first line of innate immune defense, viral proteins that render cells permissive for infection can counteract this mechanism. Certain cell types, such as HeLa cells, require the expression of the HIV-1 cofactor Vpu for particle release (Göttlinger et al., 1993; Klimkait et al., 1990; Strebel et al., 1989; Terwilliger et al., 1989), although replication occurs independently of Vpu in other cells (Gramberg et al., 2009; Strebel et al., 2009). This restriction

was attributed to the presence or absence of BST-2, also known as tetherin (or CD317 and HM1.24) (Neil et al., 2008; Van Damme et al., 2008). BST-2/tetherin was originally linked to B cell development and shown to be a marker of multiple myeloma cells (Goto et al., 1994; Masuyama et al., 2009; Ohtomo et al., 1999). Its expression is induced by IFN- α (Kawai et al., 2008), and IFN- α activation leads to HIV-1 retention at the plasma membrane in the absence of Vpu (Neil et al., 2007).

BST-2/tetherin is a type II transmembrane protein composed of a small cytosolic domain, an N-terminal transmembrane region (TMR), and an extracellular domain modified by a second membrane anchor, a C-terminal glycosyl-phosphatidylinositol (GPI) (Kupzig et al., 2003). BST-2/tetherin resides in lipid rafts at the cell surface and membranes of the *trans* Golgi network (TGN) (Kupzig et al., 2003). In HIV-1-infected cells, tetherin is retained in the TGN by Vpu (Neil et al., 2008; Van Damme et al., 2008) and targeted for endocytosis and degradation (Douglas et al., 2009; Goffinet et al., 2009; Harila et al., 2007; Mangeat et al., 2009; Mitchell et al., 2009), although it should be noted that enhancement of virus release by Vpu does not depend on downregulation or degradation of tetherin in some specific cell lines (Miyagi et al., 2009).

Inhibition of tetherin by Vpu is species specific and suggests that Vpu's activity evolved to specifically counteract human tetherin (Goffinet et al., 2009; Gupta et al., 2009; Jia et al., 2009; Sauter et al., 2009). Vpu-mediated tetherin retention requires the TMR of tetherin (McNatt et al., 2009; Rong et al., 2009) or all structural domains (Goffinet et al., 2009) and the TMR and cytosolic domain of Vpu (Van Damme et al., 2008).

The antiviral function of tetherin is not limited to HIV-1 or other retroviruses (Jouvenet et al., 2009; Zhang et al., 2009) as it also restricts release of filoviruses (Jouvenet et al., 2009; Kaletsky et al., 2009), arena viruses (Sakuma et al., 2009a), and KSHV (Bartee et al., 2006) in the absence of their respective antagonists.

Tetherin has been suggested to span both the cellular and viral membranes (Neil et al., 2008) based on its double-membrane-anchored topology (Kupzig et al., 2003), its ability to form disulfide-linked dimers (Ohtomo et al., 1999), and the presence of a predicted coiled-coil sequence in the extracellular domain. Tetherin is present in the viral membrane as a homodimer, and either TMR or the GPI anchor must be inserted into virion

envelopes for successful retention (Perez-Caballero et al., 2009). Furthermore, disulfide crosslinking via any of the three cysteines and the spacer function of the coiled coil are necessary for antiviral activity (Andrew et al., 2009; Perez-Caballero et al., 2009).

Here, we present the crystal structure of a core fragment of human tetherin, which forms a 90 Å long parallel coiled coil. The complete extracellular region adopts a ~170 Å long bent rod-like structure based on small-angle X-ray scattering analysis, defining the extracellular domain as a molecular ruler that keeps both membrane anchors at a certain distance. The coiled coil contains a number of destabilizing residues at central heptad positions, which are conserved among all known tetherin sequences. Consequently, both the core of tetherin and the complete extracellular domain show a dramatic loss in thermostability upon disulfide bond reduction *in vitro*. Mutagenesis analyses reveal that the coiled coil must be intact for function and identify an N-terminal conserved region that is required for HIV-1 restriction. The structure of tetherin explains how it can bridge long distances using a labile parallel coiled coil. Thus, tetherin has enough flexibility to insert one membrane anchor into a budding virion while the other anchor remains in the plasma membrane and excluded from the site directly involved in budding.

RESULTS

Recombinant Tetherin Forms Dimers

Recombinant tetherin(47-159) elutes from a SEC column at ~10.0 ml (Figure 1A); it migrates at ~13 kDa under reducing and at ~26 kDa under nonreducing conditions on SDS-PAGE, indicating disulfide-linked dimerization (Figure 1B). Since crystals produced from tetherin(47-159) did not diffract beyond 10 Å resolution, we applied limited trypsin proteolysis to define a smaller fragment containing residues 80-147. Tetherin(80-147) elutes from a SEC column at ~11.3 ml (Figure 1A) and reveals disulfide-linked dimerization based on SDS-PAGE analysis under reducing and nonreducing conditions (Figure 1B). In order to test whether dimerization depends mainly on disulfide-mediated crosslinking, both tetherin(47-159) and tetherin(80-147) were reduced with DTT, and cysteines were subsequently blocked with iodoacetamide; this treatment produces mostly monomeric tetherin under nonreducing SDS-PAGE conditions (Figure 1C, lanes 1 and 2). Chemical crosslinking reveals that both constructs still dimerize, as indicated by the appearance of new bands migrating at ~27 kDa (tetherin[47-159]) and between 15 and 20 kDa (tetherin[80-147]) (Figure 1C, lanes 4 and 6). Circular dichroism analyses show a high helical content (~90% helical) for both constructs (Figure 2A). Although the helical content does not change for tetherin(47-159) in the presence of DTT, tetherin(80-147) displays a reduced helical content (~70%) (Figure 2A). The effect of the reducing agent was more dramatic when thermostability was tested. While tetherin(47-159) and tetherin(80-147) show melting temperatures (T_m) of ~61°C and ~57°C, respectively, disulfide bond reduction drops the T_m to ~35°C and ~30°C, respectively (Figure 2B). The influence of disulfide bond linkage on the structure is further corroborated by the increased sensitivity of both constructs to complete degradation by trypsin treatment under reducing

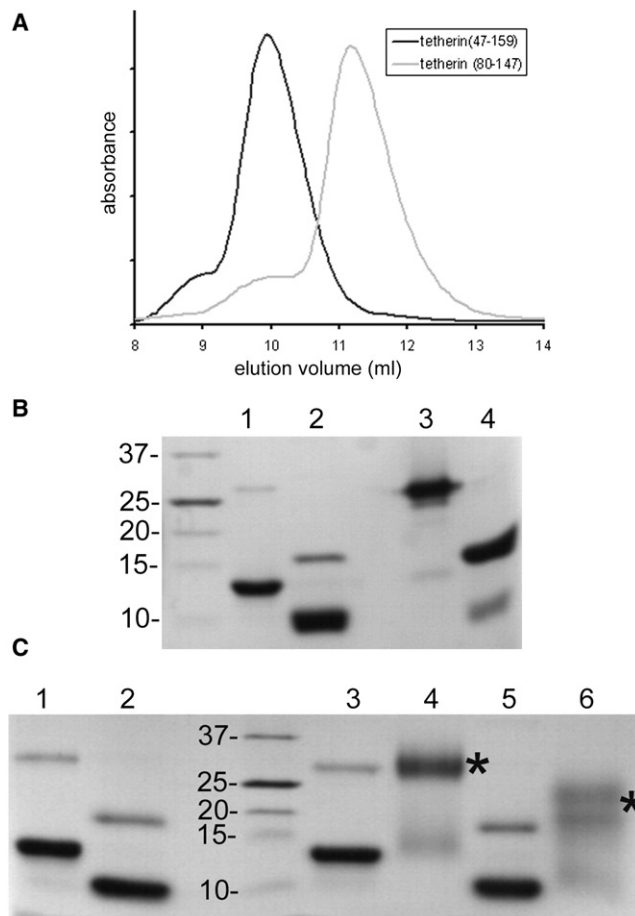


Figure 1. Biochemical Characterization of the Extracellular Domain of Tetherin

(A) SEC analysis of tetherin(47-159) and tetherin(80-147). (B) SDS-PAGE of tetherin(47-159) (lanes 1 and 3) and tetherin(80-147) under reducing (lanes 1 and 2) and nonreducing conditions (lanes 3 and 4). (C) Reduced tetherin(47-159) and tetherin(80-147) still dimerize; tetherin(47-159) (lanes 1, 3, 4) and tetherin(80-147) (lanes 2, 5, 6) were treated with iodoacetamide and separated under nonreducing conditions (lanes 1 and 2), under reducing conditions (lanes 3 and 5), and after crosslinking with 5 mM EGS (lanes 4 and 6). Dimers are indicated by *.

conditions (Figure S1). These results indicate that dimer stability greatly depends on intermolecular disulfide bonds.

Crystal Structure of Tetherin(80-147)

The crystal structure of tetherin(80-147) was determined from a selenomethionine-containing crystal using the single anomalous dispersion (SAD) method and diffraction data to 2.77 Å resolution, which produced a readily interpretable electron density map (Figure 3A). The asymmetric crystal unit contained 11 monomers that, together with crystallographic symmetry, formed six identical dimers. The best-defined dimer contains residues 89-147 and folds into a disulfide-linked 90 Å long parallel coiled coil (Figures 3B). The N-terminal residues 80-88 are disordered, and the coiled coil starts with Cys91 occupying the heptad d position followed by Val95 (a), Leu98 (d), and

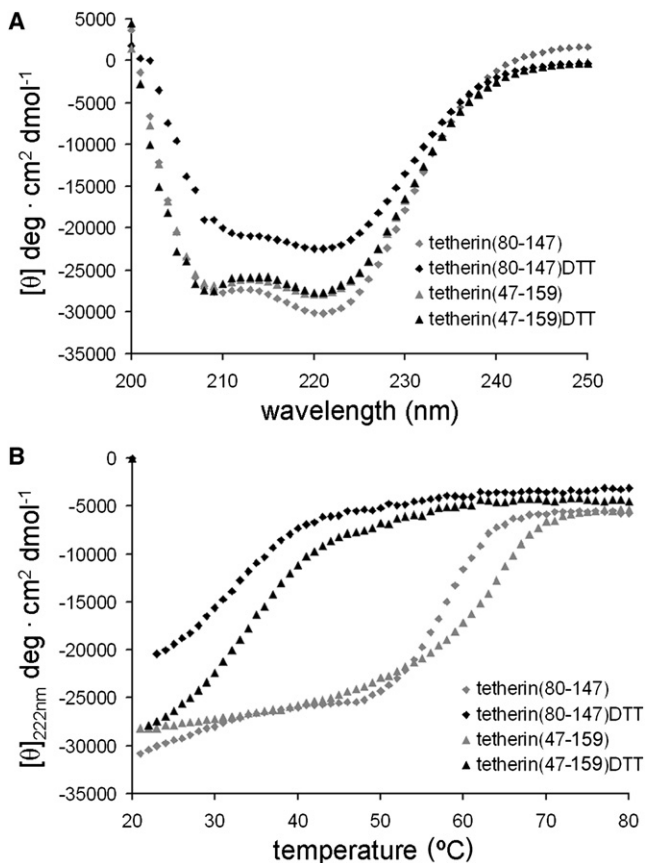


Figure 2. Disulfide Bond Reduction Decreases the Thermostability of Tetherin

(A) Circular dichroism analyses of tetherin under native and reducing conditions (DTT). Disulfide bond reduction of tetherin(80-147) reduces the overall helical content, while tetherin(47-159) is less affected.

(B) Thermostability measurements of tetherin were performed at 222 nm under native and reducing conditions (DTT), revealing a dramatic change in T_m after disulfide bond reduction.

Leu102 (a), Glu105 (d) and the stutter at Gly109 splay the coiled coil apart, documented by the increase in coiled-coil radius and pitch (Figure S2) beyond the regular coiled-coil features (Phillips, 1992). The heptad positions Val113 (a) and Leu116 (d) still show an increased coiled-coil radius and pitch (Figure S2). More regular values are adopted along the heptad positions Ile120 (a), Leu123 (d), and Leu127 (a) (Figure 3C). The irregularities that follow are produced by a stutter at Ala130, which tightens the coiled-coil radius to 4.3 Å (Figure S2), and Asn141 (d), which splay the coiled coil apart (Figures 3C and S2). Despite these irregularities, the coiled coil also contains stabilizing interactions, such as salt bridges (Glu105-Lys106, Glu133-Arg138) and an interhelical hydrogen bond (Asn141) (Figure 3C). All heptad positions are conserved among the known tetherin sequences. Modifications in some sequences include an extra helical turn before Gly100 and/or a deletion of two helical turns determined by Ala130 (a position) and Val134 (d position) (Figure S3).

The N-Terminal Extracellular Region of Tetherin Extends the Rod-like Structure

SEC analysis of tetherin(47-159) shows a larger hydrodynamic radius compared to tetherin(80-149) (Figure 1A). This is further confirmed by small-angle X-ray scattering analysis (Figure 4A). Guinier evaluation reveals radii of gyration (R_g) of 47.5 Å for tetherin(47-159) and 31.9 Å for tetherin(80-149). Maximal protein dimensions (D_{max}) of 170 Å (tetherin[47-159]) and 110 Å (tetherin[80-147]) were calculated by the distance distribution function $p(r)$ (Figure S4). The shapes of the tetherin dimers were determined ab initio, and the reconstructed models fit the experimental data with the discrepancy χ of 1.1 and 1.5, respectively (Figure 4A). The solution structure of tetherin(80-147) shows an elongated rod with dimensions of 110 × 45 × 30 Å, consistent with the 90 Å length of the rod seen in the crystal (Figure 4B). Tetherin(47-159) is more elongated and produces a rod with dimensions of 150 × 60 × 45 Å, confirming that the N-terminal region extends the coiled-coil part (Figure 4C). Part of the N terminus in the rod is slightly bent, and its orientation might be determined by the flexible linkage of the N terminus to the coiled-coil domain, as indicated by the protease sensitivity of this region (Figure S1).

The Coiled Coil and the N-Terminal Region of Tetherin Are Required for HIV-1 Retention

We next analyzed whether disruption of coiled-coil residues influences tetherin function during HIV-1 retention. Two sets of coiled-coil mutations were designed based on the crystal structure; set1 (Cys91Gly, Val95Tyr, Leu98Lys, Leu102His) disrupts the N-terminal part of the coiled coil and set2 (Leu127Lys, Ala130Tyr, Val134Glu, Leu137Glu) disrupts the C-terminal region. Recombinant forms of both mutants, tetherin(47-159)_set1 and tetherin(47-159)_set2, are soluble and elute from a SEC column in peaks overlapping with that of wild-type tetherin(47-159), indicating that the mutations change the hydrodynamic radius of the proteins (Figure S5A). The mutant proteins migrate slightly more slowly on SDS-PAGE than wild-type and reveal reduced disulfide-linked dimerization as determined under nonreducing SDS-PAGE conditions (Figure S5B). Chemical crosslinking corroborates further that the mutations interfere with dimerization; the set1 mutant shows slightly reduced dimer formation, while set2 mutant shows a more dramatic reduction in dimerization as judged by the ratio of monomer dimer bands on SDS-PAGE in comparison to wild-type tetherin(47-159) (Figure S5B). This indicates that disruption of the C-terminal coiled coil leads to a reduced detection of disulfide-linked dimers in vitro, which is most likely due to a defect in dimerization as detected by chemical crosslinking. In contrast, the set1 mutant shows only dramatically reduced disulfide-linked dimerization, although Cys53 and Cys63 are intact and could suffice to form disulfide-linked dimers (Andrew et al., 2009; Perez-Caballero et al., 2009).

Both sets of mutations were introduced into full-length tetherin containing an internal extracellular HA-tag (tetherin(iHA)) for expression in 293T cells. This indicates that tetherin(iHA)_set1 and set2 mutants are expressed on the surface of 293T cells (Figures 5C and 5D); they show membrane staining similar to that of wild-type tetherin (Neil et al., 2008) and tetherin(iHA), which appears to concentrate in patches on the plasma membrane (Figure 5B). However, expression of the full-length tetherin

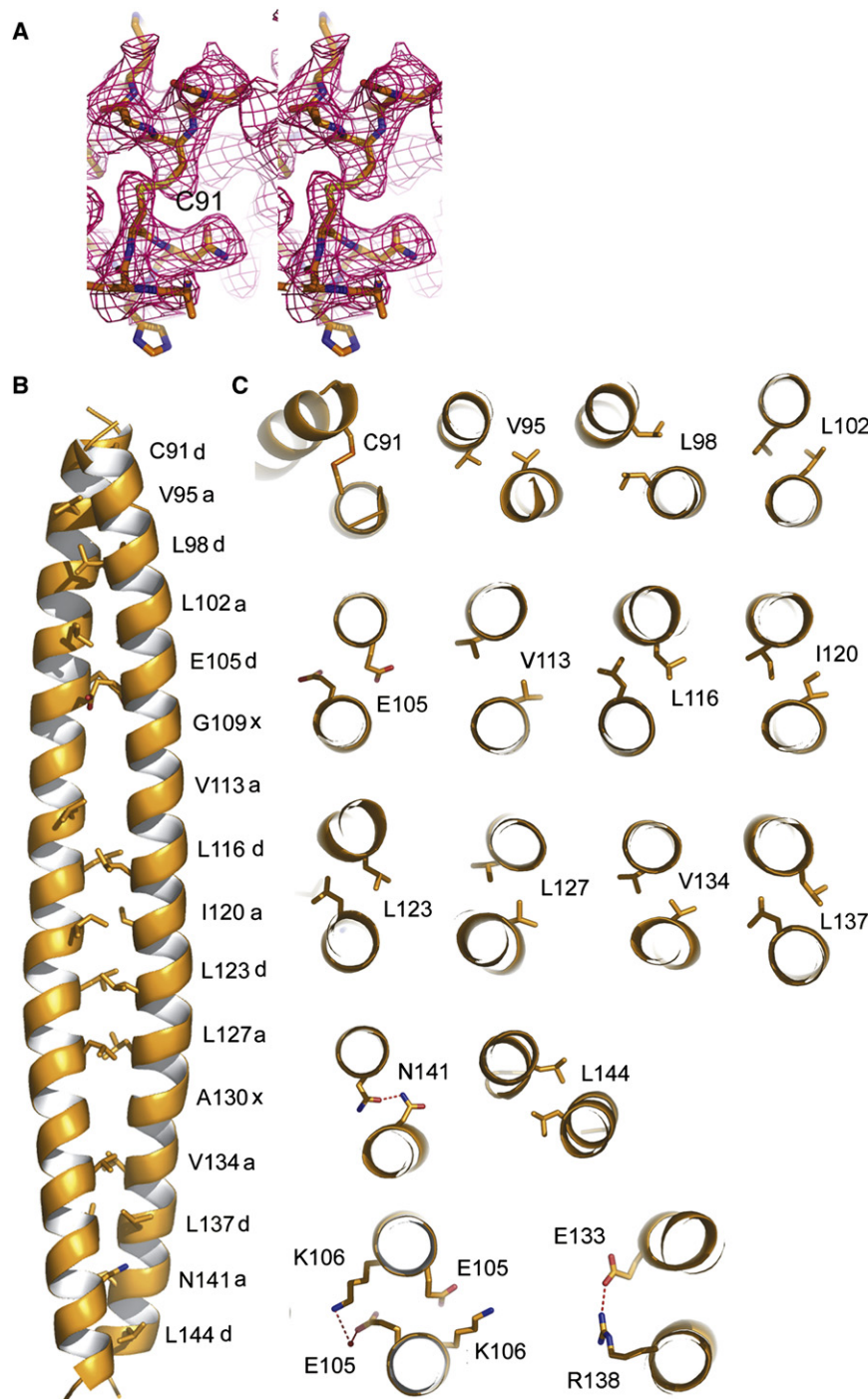


Figure 3. The Crystal Structure of Tetherin(80-147)

(A) Stereo image of the experimental electron density map obtained after SAD phasing and non-crystallographic symmetry averaging; the heptad d position occupied by Cys91 forming a disulfide bond is shown.

(B) Ribbon representation shows a 90 Å parallel coiled coil.

(C) Close-up of the heptad motifs and polar dimerization contacts.

cellular processing of Gag and were expressed at similar levels (Figure 6B, middle and right panels).

Since the extracellular region comprising residues 48–71 is highly conserved between different species (Figure S3), we tested two more sets of mutations by replacing conserved charged and polar side chains. Set3 contains changes within residues 47–58 (Lys47Ala, Asn49Gly, Glu51Ala, Arg54Ser, Asp55Ala, Arg58Ser) and set4 within residues 62–73 (Glu62Ala, Arg64Ser, Asn65Ala, His59Ser, Gln71Ala, Gln72Ala, Glu73Ser) (Figure S3). Both mutants are soluble when expressed as tetherin(47-159) and elute from a SEC column at the same position as wild-type tetherin(47-159) (Figure S6A). Furthermore, they form disulfide-linked dimers that can be efficiently crosslinked (Figure S6B). Both mutations were then introduced into full-length tetherin(iHA) and expressed in 293T cells. This demonstrates that both sets (3 and 4) of tetherin(iHA) mutants are expressed at the plasma membrane (Figures 5E and 5F). Although expression of the full-length set3 mutant reveals its activity in HIV-1 retention at a level comparable to wild-type (Figure 6B, left panel, lanes 2 and 3), expression of the set4 mutant shows no retention activity (Figure 6B, left panel, lane 4). Cells from all experiments reveal similar patterns of intracellular Gag processing (Figure 6B, middle panel). However, the extensive posttranslational modification observed

for wild-type tetherin expression in 293T cells, which generates a high molecular weight smear, is less characteristic in the case of the set4 mutant (Figure 6B, right panel, lane 4).

Since the set4 mutant includes mutagenesis of the glycosylation site at Asn65,

we constructed a single mutant of the glycosylation site at Asn65, Asn65Gln, to test whether the loss of retention activity is due to reduced glycosylation. Although the Asn65Gln mutant shows a less complex expression pattern (Figure 6C, right panel,

Cell Host & Microbe

Crystal Structure of BST-2/Tetherin

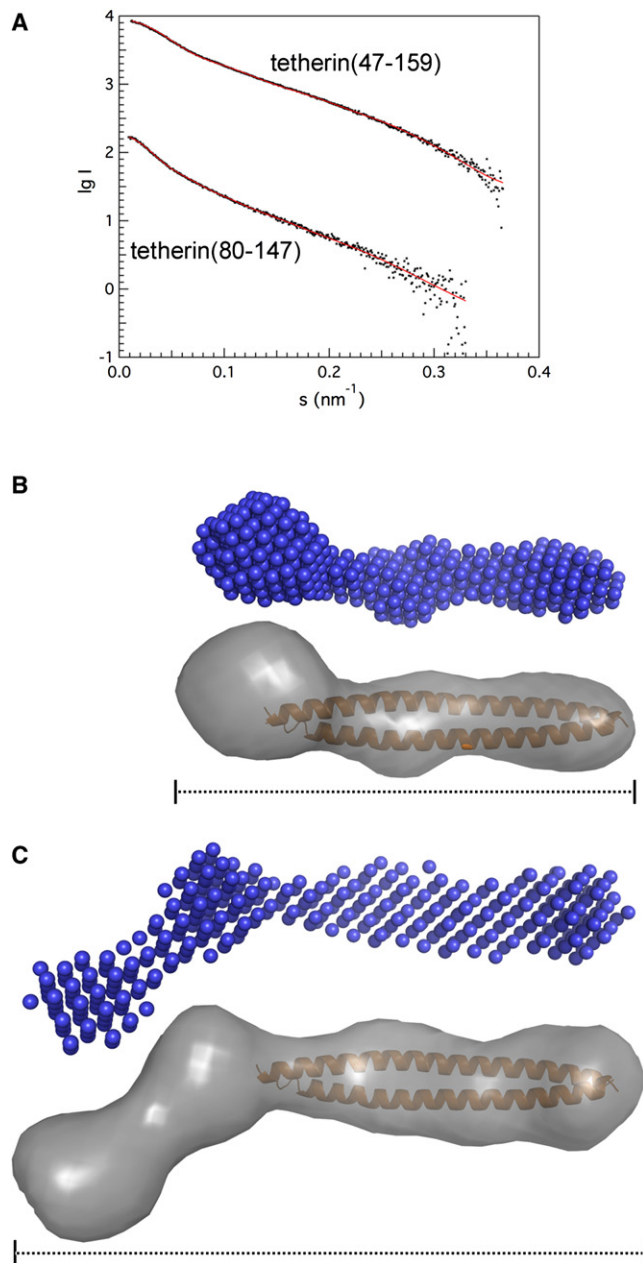


Figure 4. Small-Angle X-Ray Scattering Analysis of Tetherin

(A) Experimental scattering intensities obtained for tetherin(47-159) (upper curve) and tetherin(80-147) (lower curve) are shown as a function of resolution and after averaging and subtraction of solvent scattering. The scattering intensities calculated from representative models (presented in Figures 4B and 4C) with the lowest χ values are shown as red lines. The absolute values of the intensities of the upper curve are shifted by 2 logarithmic units.

(B and C) Ab initio models of tetherin(80-147) (B) and of tetherin(47-159) (C) reveal elongated rod-like structures; the calculated bead model as well as the molecular envelopes with the docked coiled-coil structure are shown.

lane 3), similar to tetherin_set4, the retention of HIV-1 was only slightly affected. A small amount of virus could escape, since CA was detected in the supernatant (Figure 6C, left panel, lane

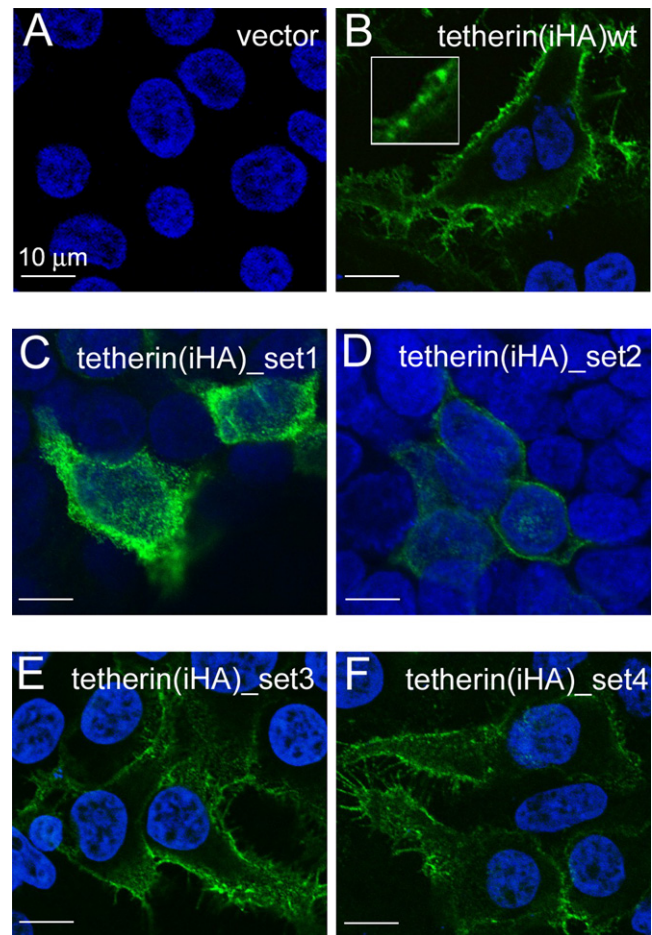


Figure 5. Cellular Localization of Wild-Type Tetherin and Mutant Forms of Tetherin

(A–F) Immunofluorescence of mock-transfected 293T cells showing DAPI staining (A); tetherin(iHA), with the inset showing a close-up of a section of the plasma membrane, revealing patches of tetherin staining (B); tetherin(iHA-set1) (C); tetherin(iHA-set2) (D); tetherin(iHA-set3) (E); and tetherin(iHA-set4) (F). All constructs reveal a similar plasma membrane staining pattern, indicating that the mutations do not affect their localization.

3). This indicates that the complete loss of retention observed for the set4 mutant is most likely not due to the changes in post-translational modification. Together, our data indicate that a conserved N-terminal region of the extracellular domain is important for tetherin function.

Since the HA-tag of tetherin(iHA) was inserted into a flexible region (Figure S3) that is disordered in the crystal structure and sensitive to proteolysis (Figure S1), we tested the effect of the insertion on tetherin function. Expression of tetherin(iHA) reveals a slightly reduced HIV-1 retention activity in comparison to wild-type tetherin, as judged by the detection of CA in the supernatant (Figure 6D, left panel, lanes 2 and 3). Both wild-type and tetherin(iHA) show similar expression patterns (Figure 6D, right panel) and accumulation of intracellular Gag as compared to the vector control (Figure 6D, middle panel). This indicates that the conformational flexibility within residues 80–88 tolerates the insertion of the

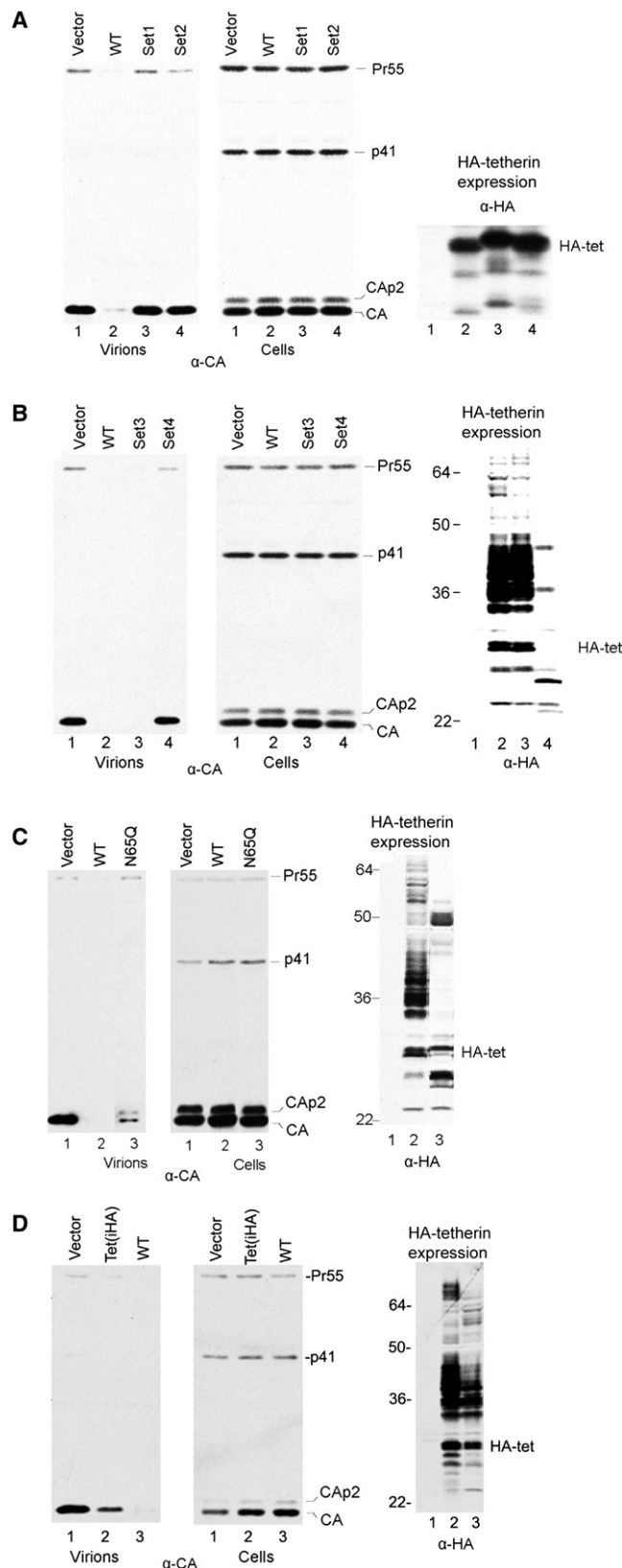


Figure 6. Mutations within the Coiled Coil and the N-Terminal Region Affect Tetherin Function during HIV-1 Retention

(A) Expression of tetherin_set1 and tetherin_set2 abolishes the retention function of tetherin. Release of virions (left panel, lanes 3 and 4) is the same as in case of the vector control (lane 1), whereas wild-type tetherin prevents virion release (left panel, lane 2). The middle panel shows that intracellular Gag and its processing are not affected by the expression of mutant tetherin (lanes 3 and 4). The right panel shows the expression levels of mutant (lanes 3 and 4) and wild-type tetherin (lane 2).

(B) Expression of tetherin_set3 (left panel) has no effect on tetherin function (lane 3) while tetherin_set4 abolishes the retention function of tetherin (lane 4), as indicated by the extracellular detection of CA. The middle panel shows that intracellular Gag and its processing are not affected by the expression of mutant tetherin (lanes 3 and 4). The right panel shows the expression levels of mutant and wild-type tetherin. Note that the extensive posttranslational modification observed for wild-type tetherin is absent in case of the set4 mutant.

(C) Expression of the tetherin mutant Asn65Gln (N65Q) (left panel) has little effect on tetherin function (lane 3) compared to wild-type tetherin (lane 2). Intracellular Gag processing is not affected by the expression of the N65Q mutant (middle panel, lanes 2 and 3). The right panel shows that the expression pattern of N65Q (lane 3) is less complex than that of wild-type tetherin (lane 2).

(D) Expression of tetherin(iHA) (left panel) has little effect on tetherin function (lane 2) when compared to wild-type tetherin (lane 3). The middle panel shows that intracellular Gag and its processing are not affected. The right panel shows the expression levels of tetherin(iHA) and wild-type tetherin.

HA-tag but slightly reduces the efficacy of HIV-1 retention. Although we lack high-resolution structural information of the N terminus, the flexible region accommodating the HA-tag might correspond to the bent conformation of tetherin(47-159) observed in the model calculated based on SAXS data (Figure 4C).

DISCUSSION

Tetherin inhibits the release of some enveloped viruses, including HIV-1, in the absence of Vpu (Neil et al., 2008) by bridging cellular and viral membranes (Perez-Caballero et al., 2009) (Fitzpatrick et al., 2010). Our structural analyses demonstrate that the complete extracellular domain of tetherin adopts an extended conformation that spans a maximal distance of 170 Å. More than half of this is provided by a 90 Å long parallel coiled coil. The low-resolution model based on X-ray scattering data indicates a slightly bent orientation of the N-terminal domain with respect to the coiled coil. This might be due to flexibility within the region (residues 79–89) connecting the N-terminal and coiled-coil domains, as documented by the sensitivity to proteolysis and the absence of an ordered structure for residues 80–88. In addition, this region permits the insertion of a HA-tag epitope without substantial loss of tetherin function.

The extracellular rod-like structure must be connected to the TMR via three N-terminal residues and to the GPI anchor via one C-terminal residue. Consequently, it is unlikely that tetherin is positioned parallel between cellular and viral membranes, which would tether virions quite close to the plasma membrane. The distance between both membranes would be less than 3–5 nm. Thin-section electron microscopy images support a larger distance between virions and the plasma membrane (Neil et al., 2008; Perez-Caballero et al., 2009). Thus, upon virion tethering, the dimeric tetherin rod has most likely one end

anchored in the plasma membrane and the other one in the virus membrane, as hypothesized (Perez-Caballero et al., 2009).

The length of the rod and its rather rigid structure in solution suggest that it functions as a molecular ruler that connects two entities via a 170 Å distance. The importance of the spacer function is documented by our mutagenesis studies of the coiled-coil region and by the deletion of the coiled coil (Perez-Caballero et al., 2009), both of which lead to a loss of the HIV-1 retention function. Such a molecular ruler function might be also required to connect adjacent lipid rafts within the plasma membrane (Kupzig et al., 2003).

Single cysteine mutations do not affect tetherin function dramatically, but mutagenesis of all three cysteines led to a complete loss of function during HIV-1 release (Andrew et al., 2009; Perez-Caballero et al., 2009), although the mutant is still active during Lassa and Marburg virus VLP release (Sakuma et al., 2009b). We show that the presence of disulfide bonds is crucial for the stability of the extracellular domain, since the T_m drops to 35°C (tetherin[47-159]) under reducing conditions. The low stability of tetherin under reducing conditions is most likely due to instability of the coiled coil, which shows an even lower T_m under reducing conditions. The coiled coil contains a number of coiled-coil-destabilizing residues occupying central heptad positions. These positions do not follow classical knobs-into-holes packing but instead loosen the coiled-coil pitch and induce an expansion of its radius. Although the coiled-coil region contains two interhelical salt bridges and one interhelical hydrogen bond, which are employed to stabilize coiled coils (Burkhard et al., 2002), the solvent exposure of the apolar heptad positions (Li et al., 2003) might contribute to the dramatic instability of the coiled coil in the absence of the disulfide bond. Together, these structural features explain the low T_m in the absence of stabilizing disulfide bonds.

This mode of labile coiled-coil interactions might serve two functions. First, tetherin's cellular function might involve the formation of heterodimers with a yet unknown ligand employing its coiled coil to form more stable dimers. Second, the weak coiled-coil interactions together with the stabilizing disulfide bonds generate a dynamic structure, which permits disassembly and reassembly of the coiled coil during dynamic processes. The latter function is in agreement with the presence of similar dynamic or destabilizing coiled-coil features in myosin (Blankenfeldt et al., 2006; Li et al., 2003), tropomyosin (Brown et al., 2001), and the streptococcus M1 protein (McNamara et al., 2008) that have been suggested to be important for their mode of action.

Despite its instability in vitro, we demonstrate the importance of the coiled coil in vivo. Mutagenesis of N- and C-terminal sets of highly conserved heptad positions eliminates the tethering function, although the mutant proteins are still expressed on the plasma membrane. This indicates that the spacer function provided by proper coiled-coil formation is essential for tethering. We also identified a third set of residues within the highly conserved N-terminal extracellular region that are functionally required. Mutations within the stretch of residues 48–59 have no effect on tethering, whereas changes within residues 62–73 lead to a loss of the tethering function. Again, both mutant proteins are expressed on the plasma membrane, and the extracellular domains form dimers in vitro. Since the set4 mutant eliminates the glycosylation site at Asn65 and shows a less complex

expression pattern than wild-type tetherin, we tested whether changes in posttranslational modification are responsible for loss of tetherin function. Although the expression pattern of Asn65Gln resembles that of the set4 mutant, it shows only slightly reduced HIV-1 retention activity, consistent with previous findings reporting no effect on HIV-1 retention of single and double glycosylation mutants of tetherin (Andrew et al., 2009). This indicates that mutagenesis of this N-terminal region (set4) either affects its spacer function or eliminates an important docking site, possibly for self-assembly. Although Perez-Caballero et al. reported that the N terminus can be replaced by a similar region derived from the transferrin receptor and the coiled coil can be replaced by the dystrophin myotonic protein kinase coiled coil, it is important to note that the activity of art-tetherin is ~10-fold lower (Perez-Caballero et al., 2009). In contrast, our data clearly demonstrate that the N-terminal domain and the dynamic features of the coiled coil of tetherin are essential for HIV-1 retention.

Based on our structural analysis, we propose the following interplay between the elongated shape and the conformational flexibility of tetherin. Although we do not know at which stage of assembly tetherin enters the virion membrane, it is likely that it is present from the beginning of assembly starting from lipid rafts. Since virus assembly and budding is a dynamic process, tetherin cannot remain too rigid. The coiled-coil instabilities thus permit a certain degree of flexibility for the tetherin dimers to diffuse laterally into the budding site with four membrane anchors while maintaining the strict distance between the membrane anchors. The conformational flexibility, which entails most likely opening and reassembly of the coiled coil, is facilitated by the presence of the disulfide bonds. Consequently, dimer dissociation and restabilization do not interfere with the dynamic process of virus assembly and budding, and tetherin remains anchored in the newly formed viral membrane, maintaining its spacer function. Furthermore, the elongated rod-like structure might be involved in self-assembly, as supported by the punctate appearance of tetherin in the plasma membrane. Such clustering might require an intact N-terminal region, which could cluster tetherin around the membrane neck of a budding virion, consistent with the accumulation of tetherin at HIV-1 budding sites (Habermann et al., 2010). This would ensure that at least one or several tetherin dimers can efficiently insert into the viral membrane to render the system efficient. Finally, the structural basis, which controls tetherin incorporation into virions even in the presence of Vpu in some cells without restriction of HIV-1 release (Fitzpatrick et al., 2010), may depend on its surface density (Habermann et al., 2010) but remains to be determined.

EXPERIMENTAL PROCEDURES

Bacterial Protein Expression and Purification

cDNA encoding human tetherin/BST-2 residues 47–159 and 80–147 was cloned into expression vector pETM11. Site-directed mutagenesis of tetherin (47–159) was carried out using standard protocols and verified by sequencing. Protein expression was performed in *E. coli* Rosetta2 cells induced with isopropyl β-D-1-thiogalactopyranoside (IPTG) at 20°C for 4 hr. Cells were lysed in buffer A (20 mM Tris [pH 8.0], 0.1 M NaCl, 10 mM imidazole), and proteins were purified by Ni²⁺ chromatography. The His-tag was removed by tobacco etch virus (TEV) protease cleavage, and both TEV and uncleaved protein were removed by Ni²⁺ chromatography. Final purification steps included anion-exchange chromatography (mono Q; GE Healthcare; Waukesha, WI) in

buffer B (20 mM bicine [pH 9.3], 0.1 M NaCl, 5 mM EDTA) and size-exclusion chromatography (Superdex 75; GE Healthcare) in buffer C (20 mM HEPES [pH 8.0], 0.1 M NaCl, 5 mM EDTA). Selenomethionine-substituted tetherin(80-147) and mutant tetherin proteins were purified as described above. Mutant tetherin constructs contain the following mutations: tetherin_set1, Cys91Gly, Val95Tyr, Leu98Lys, Leu102His; tetherin_set2, Leu127Lys, Ala130-Tyr, Val134Glu, Leu137Glu; tetherin_set3, Lys47Ala, Asn49Gly, Glu51Ala, Arg54Ser, Asp55Ala, Arg58Ser; tetherin_set4, Glu62Ala, Arg64Ser, Asn65Ala, His59Ser, Gln71Ala, Gln72Ala, Glu73Ser.

Crystallization, Data Collection, and Structure Solution

Tetherin(80-147) was crystallized at a concentration of 5 mg/ml by mixing 1 μ l protein and 1 μ l reservoir solution (0.02 M MgCl₂, 0.1 M bis tris [pH 5.0], 20% polyacrylic acid) at 20°C. Crystals were cryoprotected in reservoir solution supplemented by 26% glycerol and flash-frozen in liquid nitrogen. A SAD data set was collected at ESRF (Grenoble, France), beamline ID14-4. Data were indexed and processed with XDS (Kabsch, 1993) and scaled with SCALA (CCP4, 1994; Evans, 2006). The crystals belong to space group C2 with unit cell dimensions of a = 169.89Å, b = 85.93Å, c = 123.31Å, and β = 126.94° and contain 11 monomers per asymmetric unit.

Heavy-atom positions were located with SHELXD (Schneider and Sheldrick, 2002), and the correct hand was verified using SHELXE (Sheldrick, 2002). The experimental phases were calculated using SHARP (Bricogne et al., 2003) and resulted in an overall figure of merit (FOM) of 0.38/0.10 for the acentric and centric reflections, respectively. These phases were improved using a 70% solvent content in SOLOMON (Abrahams and Leslie, 1996). An initial model was built using RESOLVE (Terwilliger and Berendzen, 1999), which allowed the determination of the noncrystallographic symmetry operators. The electron density map was further improved using 11-fold averaging, and the final model was built manually using the program COOT (Emsley and Cowtan, 2004). The structure was refined to a resolution of 2.77 Å with the program PHENIX (Adams et al., 2002), with an R_{factor} of 0.24 and R_{free} of 0.27 with good stereochemistry (Table 1). Most (96.88%) of the residues are within the preferred and allowed regions of a Ramachandran plot (CCP4, 1994). Chains A, F, I, and J contain amino acids (aa) 89–147; chain B, aa 89–145; chain C, aa 89–137; chain D, aa 87–142; chain E, aa 88–146; chain G, aa 88–141; chain H, aa 89–142; and chain K, aa 89–127. Molecular graphics figures were generated with PyMOL (<http://www.pymol.org>). The helical parameters of the coiled coil were calculated using the program TWISTER (Strelkov and Burkhard, 2002).

Biophysical and Biochemical Characterization of Tetherin

CD spectroscopy measurements were performed using a JASCO Inc. (Easton, MD) spectropolarimeter equipped with a thermoelectric temperature controller. Spectra of each sample were recorded at 20°C in buffer D (20 mM phosphate [pH 7], 100 mM NaCl). For thermal denaturation experiments, the ellipticity was recorded at 222 nm with 1°C steps from 20°C to 100°C, with a slope of 1°C/min. Ellipticity values were converted to mean residue ellipticity.

Proteolysis of tetherin was carried out in buffer C at room temperature (RT) with a trypsin-to-protein ratio of 1:100 (w/w). Dimerization of tetherin under reducing conditions was tested as follows: Proteins were reduced with 10 mM DTT and subsequently incubated with 100 mM iodoacetamide at RT for 1 hr. Unbound DTT and iodoacetamide were removed by dialysis in buffer C, and samples were crosslinked with 5 mM ethylene glycol bis(succinimidyl succinate) (EGS). The crosslinking reaction was quenched with 20 mM Tris (pH 8.0).

Small-Angle X-Ray Scattering Analysis

X-ray scattering data were collected on ESRF (Grenoble) beamline ID14-EH3 at a sample-detector distance of 2.4 m covering a range of momentum transfer of $0.1 < s < 4.5 \text{ nm}^{-1}$ ($s = 4\pi \sin(\theta)/\lambda$, where θ is the scattering angle and $\lambda = 0.15 \text{ nm}$ is the X-ray wavelength). The scattering intensity of tetherin(47-159) was measured at protein concentrations of 2 and 13 mg/ml and that of tetherin(80-147) at concentrations of 2 and 11 mg/ml in buffer C. The data were normalized to the intensity of the incident beam; the scattering of the buffer was subtracted and the resulting intensities were scaled for concentration. Data processing was performed using the program package PRIMUS (Konarev et al., 2003). The forward scattering, $I(0)$, and the R_g were calculated

Table 1. Crystallographic Statistics

Data Collection Statistics	
Space group	C2
Cell dimensions a, b, c; β	169.89 Å, 85.93 Å, 123.31 Å; 126.94°
Wavelength (Å)	0.979
Resolution (Å)	45.00–2.77 (2.92–2.77)
R _{merge}	0.086 (0.479)
Completeness (%)	98.1 (97.7)
I/ σ (I)	13.8 (3.8)
Redundancy	7.6 (7.7)
Refinement Statistics	
Resolution range (Å)	44.8–2.77
No. reflections	35,361
R _{work} /R _{free}	0.2407/0.2737
No. protein atoms	4596
No. of ligands/ion	21
No. of waters	126
B factors protein/ligand/water	88.56/62.65/66.31
Rmsd (bonds) (Å)	0.014
Rmsd (angles) (°)	1.305
Values in parentheses are for highest-resolution shell.	

with GNOM, which also provides the distance distribution function, $p(r)$, of the particle (Svergun, 1992). Low-resolution models of both tetherin samples were simulated by the program DAMMIN (Svergun, 1999) and GASBOR (Svergun et al., 2001), which resulted in similar elongated structures. Figure 4 represents the GASBOR model. The crystal structure of tetherin(80-147) was docked into the low-resolution models using the program package SITUS (Wriggers et al., 1999).

Mammalian Expression Constructs and HIV-1 Release Assay

The coding sequence for full-length human tetherin with an N-terminal HA-tag (HA-tetherin) or an HA-tag inserted into the extracellular domain between residues Gln82 and Asp83 (tetherin[iHA]) was cloned into the mammalian expression vector pBJ5. To examine the effects of WT and mutant tetherin on HIV-1 release, 293T cells (1.2×10^6) were seeded into T25 flasks and transfected 24 hr later using a calcium phosphate precipitation technique. The cultures were transfected with 1 μ g Vpu-negative proviral DNA (HIV-1_{HXB2}) together with expression vectors for WT or mutant HA-tetherin or the empty vector (50 ng). The total amount of transfected DNA was brought to 8 μ g with carrier DNA (pTZ18U). Twenty-four hours posttransfection, the cells were lysed in radioimmunoprecipitation assay buffer (140 mM NaCl, 8 mM Na₂HPO₄, 2 mM NaH₂PO₄, 1% NP-40, 0.5% sodium deoxycholate, 0.05% SDS), and the culture supernatants were clarified by low-speed centrifugation and passed through 0.45 μ m filters. Virions released into the medium were pelleted through 20% sucrose cushions by ultracentrifugation for 2 hr at 27,000 rpm and 4°C in a Beckman SW41 rotor. Pelletable material and the cell lysates were analyzed by SDS-PAGE and western blotting, using the anti-HIV CA antibody 183-H12-5C (Chesebro et al., 1992) to detect Gag proteins. HA-tagged tetherin was detected with the anti-HA mouse monoclonal antibody HA.11.

Immunofluorescence Analysis

Tetherin expression vectors containing the extracellular internal HA-tag were transfected into 293T cells using standard methods. For indirect immunofluorescence (IIF), 293T cells were cultured on coverslips and fixed with 4% paraformaldehyde for 20 min at 4°C. The coverslips were incubated with an α HA-tag antibody in PBS for 1 hr at RT. Slides were washed three times with PBS, followed by the secondary antibody incubation at RT for 1 hr (Alexa

Cell Host & Microbe

Crystal Structure of BST-2/Tetherin

488- or 594-coupled anti-mouse or anti-rabbit goat antibodies in PBS). After three washes with PBS, slides were mounted in Mowiol and analyzed by confocal microscopy.

ACCESSION NUMBERS

Coordinates and structure factors have been deposited in the Protein Data Bank with accession number 2x7a.

SUPPLEMENTAL INFORMATION

Supplemental Information includes six figures and can be found with this article online at doi:10.1016/j.chom.2010.03.005.

ACKNOWLEDGMENTS

This work was supported by the Agence Nationale de la Recherche (ANR-08-BLAN-0271-01 to W.W.), the Deutsche Forschungsgemeinschaft (DFG SPP1175 to W.W.), the National Institute of Allergy and Infectious Diseases (R37AI029873 to H.G.), and a postdoctoral fellowship from the European Molecular Biology Organization (B.H.). We thank S. Avilov for help with confocal microscopy and B. Connell for characterization of the first tetherin constructs. We acknowledge the Partnership for Structural Biology (<http://www.psb-grenoble.eu>) for access to the common platforms, including the crystallization facility (J. Marquez), and the ESRF and EMBL for beam time and assistance during data collection. The following reagent was obtained through the AIDS Research and Reference Reagent Program, Division of AIDS, NIAID, NIH: HIV-1 p24 monoclonal antibody (183-H12-5C) from Bruce Chesebro and Kathy Wehrly.

Received: December 18, 2009

Revised: February 11, 2010

Accepted: March 8, 2010

Published online: April 15, 2010

REFERENCES

Abrahams, J.P., and Leslie, A.G. (1996). Methods used in the structure determination of bovine mitochondrial F1 ATPase. *Acta Crystallogr. D Biol. Crystallogr.* 52, 30–42.

Adams, P.D., Grosse-Kunstleve, R.W., Hung, L.-W., Ioerger, T.R., McCoy, A.J., Moriarty, N.W., Read, R.J., Sacchettini, J.C., Sauter, N.K., and Terwilliger, T.C. (2002). PHENIX: building new software for automated crystallographic structure determination. *Acta Crystallogr. D Biol. Crystallogr.* 58, 1948–1954.

Andrew, A.J., Miyagi, E., Kao, S., and Strebel, K. (2009). The formation of cysteine-linked dimers of BST-2/tetherin is important for inhibition of HIV-1 virus release but not for sensitivity to Vpu. *Retrovirology* 6, 80.

Bartee, E., McCormack, A., and Früh, K. (2006). Quantitative membrane proteomics reveals new cellular targets of viral immune modulators. *PLoS Pathog.* 2, e107.

Blankenfeldt, W., Thomä, N.H., Wray, J.S., Gautel, M., and Schlichting, I. (2006). Crystal structures of human cardiac beta-myosin II S2-Delta provide insight into the functional role of the S2 subfragment. *Proc. Natl. Acad. Sci. USA* 103, 17713–17717.

Bricogne, G., Vonrhein, C., Flensburg, C., Schiltz, M., and Paciorek, W. (2003). Generation, representation and flow of phase information in structure determination: recent developments in and around SHARP 2.0. *Acta Crystallogr. D Biol. Crystallogr.* 59, 2023–2030.

Brown, J.H., Kim, K.H., Jun, G., Greenfield, N.J., Dominguez, R., Volkman, N., Hitchcock-DeGregori, S.E., and Cohen, C. (2001). Deciphering the design of the tropomyosin molecule. *Proc. Natl. Acad. Sci. USA* 98, 8496–8501.

Burkhard, P., Ivaninskii, S., and Lustig, A. (2002). Improving coiled coil stability by optimizing ionic interactions. *J. Mol. Biol.* 318, 901–910.

CCP4 (Collaborative Computational Project, Number 4) (1994). The CCP4 suite: programs for protein crystallography. *Acta Crystallogr. D Biol. Crystallogr.* 50, 760–763.

Chesebro, B., Wehrly, K., Nishio, J., and Perryman, S. (1992). Macrophage-tropic human immunodeficiency virus isolates from different patients exhibit unusual V3 envelope sequence homogeneity in comparison with T-cell-tropic isolates: definition of critical amino acids involved in cell tropism. *J. Virol.* 66, 6547–6554.

Douglas, J.L., Viswanathan, K., McCarroll, M.N., Gustin, J.K., Früh, K., and Moses, A.V. (2009). Vpu directs the degradation of the human immunodeficiency virus restriction factor BST-2/Tetherin via a betaTrCP-dependent mechanism. *J. Virol.* 83, 7931–7947.

Emsley, P., and Cowtan, K. (2004). Coot: model-building tools for molecular graphics. *Acta Crystallogr. D Biol. Crystallogr.* 60, 2126–2132.

Evans, P. (2006). Scaling and assessment of data quality. *Acta Crystallogr. D Biol. Crystallogr.* 62, 72–82.

Fitzpatrick, K., Skasko, M., Deerinck, T.J., Crum, J., Ellisman, M.H., and Guatelli, J. (2010). Direct restriction of virus release and incorporation of the interferon-induced protein BST-2 into HIV-1 particles. *PLoS Pathog.* 6, e1000701.

Goffinet, C., Allespach, I., Homann, S., Tervo, H.M., Habermann, A., Rupp, D., Oberbremer, L., Kern, C., Tibroni, N., Welsch, S., et al. (2009). HIV-1 antagonism of CD317 is species specific and involves Vpu-mediated proteasomal degradation of the restriction factor. *Cell Host Microbe* 5, 285–297.

Goto, T., Kennel, S.J., Abe, M., Takishita, M., Kosaka, M., Solomon, A., and Saito, S. (1994). A novel membrane antigen selectively expressed on terminally differentiated human B cells. *Blood* 84, 1922–1930.

Göttlinger, H.G., Dorfman, T., Cohen, E.A., and Haseltine, W.A. (1993). Vpu protein of human immunodeficiency virus type 1 enhances the release of capsids produced by gag gene constructs of widely divergent retroviruses. *Proc. Natl. Acad. Sci. USA* 90, 7381–7385.

Gramberg, T., Sunseri, N., and Landau, N.R. (2009). Accessories to the crime: recent advances in HIV accessory protein biology. *Curr. HIV/AIDS Rep.* 6, 36–42.

Gupta, R.K., Hué, S., Schaller, T., Verschoor, E., Pillay, D., and Towers, G.J. (2009). Mutation of a single residue renders human tetherin resistant to HIV-1 Vpu-mediated depletion. *PLoS Pathog.* 5, e1000443.

Habermann, A., Krijnse Locker, J., Oberwinkler, H., Eckhardt, M., Homann, S., Andrew, A., Strebel, K., and Kräusslich, H.-G. (2010). CD317/Tetherin is enriched in the HIV-1 envelope 1 and downregulated from the plasma membrane upon virus infection. *J. Virol.*, in press. Published online February 10, 2010. 10.1128/JVI.02421-09.

Harila, K., Salminen, A., Prior, I., Hinkula, J., and Suomalainen, M. (2007). The Vpu-regulated endocytosis of HIV-1 Gag is clathrin-independent. *Virology* 369, 299–308.

Jia, B., Serra-Moreno, R., Neidermyer, W., Rahmberg, A., Mackey, J., Fofana, I.B., Johnson, W.E., Westmoreland, S., and Evans, D.T. (2009). Species-specific activity of SIV Nef and HIV-1 Vpu in overcoming restriction by tetherin/BST2. *PLoS Pathog.* 5, e1000429.

Jouvenet, N., Neil, S.J., Zhadina, M., Zang, T., Kratovac, Z., Lee, Y., McNatt, M., Hatzioannou, T., and Bieniasz, P.D. (2009). Broad-spectrum inhibition of retroviral and filoviral particle release by tetherin. *J. Virol.* 83, 1837–1844.

Kabsch, W. (1993). Automatic processing of rotation diffraction data from crystals of initially unknown symmetry and cell constants. *J. Appl. Cryst.* 26, 795–800.

Kaletsky, R.L., Francica, J.R., Agrawal-Gamse, C., and Bates, P. (2009). Tetherin-mediated restriction of filovirus budding is antagonized by the Ebola glycoprotein. *Proc. Natl. Acad. Sci. USA* 106, 2886–2891.

Kawai, S., Azuma, Y., Fujii, E., Furugaki, K., Ozaki, S., Matsumoto, T., Kosaka, M., and Yamada-Okabe, H. (2008). Interferon-alpha enhances CD317 expression and the antitumor activity of anti-CD317 monoclonal antibody in renal cell carcinoma xenograft models. *Cancer Sci.* 99, 2461–2466.

- Klimkait, T., Strebel, K., Hoggan, M.D., Martin, M.A., and Orenstein, J.M. (1990). The human immunodeficiency virus type 1-specific protein vpu is required for efficient virus maturation and release. *J. Virol.* **64**, 621–629.
- Konarev, P.V., Volkov, V.V., Sokolova, A.V., Koch, M.H.J., and Svergun, D.I. (2003). PRIMUS: a Windows PC-based system for small-angle scattering data analysis. *J. Appl. Cryst.* **36**, 1277–1282.
- Kupzig, S., Korolchuk, V., Rollason, R., Sugden, A., Wilde, A., and Banting, G. (2003). Bst-2/HM1.24 is a raft-associated apical membrane protein with an unusual topology. *Traffic* **4**, 694–709.
- Li, Y., Brown, J.H., Reshetnikova, L., Blazsek, A., Farkas, L., Nyitrai, L., and Cohen, C. (2003). Visualization of an unstable coiled coil from the scallop myosin rod. *Nature* **424**, 341–345.
- Malim, M.H., and Emerman, M. (2008). HIV-1 accessory proteins—ensuring viral survival in a hostile environment. *Cell Host Microbe* **3**, 388–398.
- Mangeat, B., Gers-Huber, G., Lehmann, M., Zufferey, M., Luban, J., and Piguet, V. (2009). HIV-1 Vpu neutralizes the antiviral factor Tetherin/BST-2 by binding it and directing its beta-TrCP2-dependent degradation. *PLoS Pathog.* **5**, e1000574.
- Masuyama, N., Kuronita, T., Tanaka, R., Muto, T., Hirota, Y., Takigawa, A., Fujita, H., Aso, Y., Amano, J., and Tanaka, Y. (2009). HM1.24 is internalized from lipid rafts by clathrin-mediated endocytosis through interaction with alpha-adaptin. *J. Biol. Chem.* **284**, 15927–15941.
- McNamara, C., Zinkernagel, A.S., Macheboeuf, P., Cunningham, M.W., Nizet, V., and Ghosh, P. (2008). Coiled coil irregularities and instabilities in group A *Streptococcus* M1 are required for virulence. *Science* **319**, 1405–1408.
- McNatt, M.W., Zang, T., Hatzioannou, T., Bartlett, M., Fofana, I.B., Johnson, W.E., Neil, S.J., and Bieniasz, P.D. (2009). Species-specific activity of HIV-1 Vpu and positive selection of tetherin transmembrane domain variants. *PLoS Pathog.* **5**, e1000300.
- Mitchell, R.S., Katsura, C., Skasko, M.A., Fitzpatrick, K., Lau, D., Ruiz, A., Stephens, E.B., Margottin-Gouget, F., Benarous, R., and Guatelli, J.C. (2009). Vpu antagonizes BST-2-mediated restriction of HIV-1 release via beta-TrCP and endo-lysosomal trafficking. *PLoS Pathog.* **5**, e1000450.
- Miyagi, E., Andrew, A.J., Kao, S., and Strebel, K. (2009). Vpu enhances HIV-1 virus release in the absence of Bst-2 cell surface down-modulation and intracellular depletion. *Proc. Natl. Acad. Sci. USA* **106**, 2868–2873.
- Neil, S.J., Sandrin, V., Sundquist, W.I., and Bieniasz, P.D. (2007). An interferon-alpha-induced tethering mechanism inhibits HIV-1 and Ebola virus particle release but is counteracted by the HIV-1 Vpu protein. *Cell Host Microbe* **2**, 193–203.
- Neil, S.J., Zang, T., and Bieniasz, P.D. (2008). Tetherin inhibits retrovirus release and is antagonized by HIV-1 Vpu. *Nature* **451**, 425–430.
- Ohtomo, T., Sugamata, Y., Ozaki, Y., Ono, K., Yoshimura, Y., Kawai, S., Koishihara, Y., Ozaki, S., Kosaka, M., Hirano, T., and Tsuchiya, M. (1999). Molecular cloning and characterization of a surface antigen preferentially over-expressed on multiple myeloma cells. *Biochem. Biophys. Res. Commun.* **258**, 583–591.
- Perez-Caballero, D., Zang, T., Ebrahimi, A., McNatt, M.W., Gregory, D.A., Johnson, M.C., and Bieniasz, P.D. (2009). Tetherin inhibits HIV-1 release by directly tethering virions to cells. *Cell* **139**, 499–511.
- Phillips, G.N., Jr. (1992). What is the pitch of the α -helical coiled coil? *Proteins* **14**, 425–429.
- Rong, L., Zhang, J., Lu, J., Pan, Q., Lorgeoux, R.P., Aloysius, C., Guo, F., Liu, S.L., Wainberg, M.A., and Liang, C. (2009). The transmembrane domain of BST-2 determines its sensitivity to down-modulation by human immunodeficiency virus type 1 Vpu. *J. Virol.* **83**, 7536–7546.
- Sakuma, T., Noda, T., Urata, S., Kawaoka, Y., and Yasuda, J. (2009a). Inhibition of Lassa and Marburg virus production by tetherin. *J. Virol.* **83**, 2382–2385.
- Sakuma, T., Sakurai, A., and Yasuda, J. (2009b). Dimerization of tetherin is not essential for its antiviral activity against Lassa and Marburg viruses. *PLoS ONE* **4**, e6934.
- Sauter, D., Schindler, M., Specht, A., Landford, W.N., Münch, J., Kim, K.-A., Votteler, J., Schubert, U., Bibollet-Ruche, F., Keele, B.F., et al. (2009). Tetherin-driven adaptation of Vpu and Nef function and the evolution of pandemic and nonpandemic HIV-1 strains. *Cell Host Microbe* **6**, 409–421.
- Schneider, T.R., and Sheldrick, G.M. (2002). Substructure solution with SHELXD. *Acta Crystallogr. D Biol. Crystallogr.* **58**, 1772–1779.
- Sheldrick, G.M. (2002). Macromolecular phasing with SHELXE. *Z. Kristallogr.* **217**, 644–650.
- Strebel, K., Klimkait, T., Maldarelli, F., and Martin, M.A. (1989). Molecular and biochemical analyses of human immunodeficiency virus type 1 vpu protein. *J. Biochem.* **378**, 3784–3791.
- Strebel, K., Luban, J., and Jeang, K.T. (2009). Human cellular restriction factors that target HIV-1 replication. *BMC Med.* **7**, 48.
- Strelkov, S.V., and Burkhard, P. (2002). Analysis of alpha-helical coiled coils with the program TWISTER reveals a structural mechanism for stutter compensation. *J. Struct. Biol.* **137**, 54–64.
- Svergun, D.I. (1992). Determination of the regularization parameter in indirect-transform methods using perceptual criteria. *J. Appl. Cryst.* **25**, 495–503.
- Svergun, D.I. (1999). Restoring low resolution structure of biological macromolecules from solution scattering using simulated annealing. *Biophys. J.* **76**, 2879–2886.
- Svergun, D.I., Petoukhov, M.V., and Koch, M.H. (2001). Determination of domain structure of proteins from X-ray solution scattering. *Biophys. J.* **80**, 2946–2953.
- Terwilliger, T.C., and Berendzen, J. (1999). Automated MAD and MIR structure solution. *Acta Crystallogr. D Biol. Crystallogr.* **55**, 849–861.
- Terwilliger, E.F., Cohen, E.A., Lu, Y.C., Sodroski, J.G., and Haseltine, W.A. (1989). Functional role of human immunodeficiency virus type 1 vpu. *Proc. Natl. Acad. Sci. USA* **86**, 5163–5167.
- Van Damme, N., Goff, D., Katsura, C., Jorgenson, R.L., Mitchell, R., Johnson, M.C., Stephens, E.B., and Guatelli, J. (2008). The interferon-induced protein BST-2 restricts HIV-1 release and is downregulated from the cell surface by the viral Vpu protein. *Cell Host Microbe* **3**, 245–252.
- Wriggers, W., Milligan, R.A., and McCammon, J.A. (1999). Situs: A package for docking crystal structures into low-resolution maps from electron microscopy. *J. Struct. Biol.* **125**, 185–195.
- Zhang, F., Wilson, S.J., Landford, W.C., Virgen, B., Gregory, D., Johnson, M.C., Munch, J., Kirchhoff, F., Bieniasz, P.D., and Hatzioannou, T. (2009). Nef proteins from simian immunodeficiency viruses are tetherin antagonists. *Cell Host Microbe* **6**, 54–67.